© 2021. Published by The Company of Biologists Ltd | Development (2021) 148, dev194027. doi:10.1242/dev.194027

STEM CELLS AND REGENERATION

RESEARCH ARTICLE

The long noncoding RNA *Meg3* regulates myoblast plasticity and muscle regeneration through epithelial-mesenchymal transition

Tiffany L. Dill, Alina Carroll, Amanda Pinheiro, Jiachen Gao and Francisco J. Naya*

ABSTRACT

Formation of skeletal muscle is among the most striking examples of cellular plasticity in animal tissue development, and while muscle progenitor cells are reprogrammed by epithelial-mesenchymal transition (EMT) to migrate during embryonic development, the regulation of EMT in post-natal myogenesis remains poorly understood. Here, we demonstrate that the long noncoding RNA (lncRNA) *Meg3* regulates EMT in myoblast differentiation and skeletal muscle regeneration. Chronic inhibition of *Meg3* in C2C12 myoblasts induced EMT, and suppressed cell state transitions required for differentiation. Furthermore, adenoviral *Meg3* knockdown compromised muscle regeneration, which was accompanied by abnormal mesenchymal gene expression and interstitial cell proliferation. Transcriptomic and pathway analyses of *Meg3*-depleted C2C12 myoblasts and injured skeletal muscle revealed a significant dysregulation of EMT-related genes, and identified TGFβ as a key upstream regulator. Importantly, inhibition of TGFβR1 and its downstream effectors, and the EMT transcription factor Snai2, restored many aspects of myogenic differentiation in *Meg3*-depleted myoblasts *in vitro*. We further demonstrate that reduction of *Meg3*-dependent Ezh2 activity results in epigenetic alterations associated with TGFβ activation. Thus, *Meg3* regulates myoblast identity to facilitate progression into differentiation.

KEY WORDS: Muscle differentiation, Cell identity, Regeneration, *Meg3*, Long noncoding RNA, Epithelial-mesenchymal transition, TGFβ

INTRODUCTION

During developmental myogenesis, polarized epithelial cells within mesoderm-derived somites undergo dramatic changes in cell identity through epithelial-mesenchymal transition (EMT) to generate muscle progenitors with the ability to migrate and ultimately fuse to form multinucleated myotubes (Yusuf and Brand-Saberi, 2006; Buckingham and Rigby, 2014; Chal and Pourquié, 2017). Similarly, repair of damaged or diseased skeletal muscle requires extensive cell state transitions in muscle and non-muscle progenitors, which collaborate to form newly functional myofibers (Uezumi et al., 2014; Wosczyna and Rando, 2018). The temporal control of EMT in both embryonic and regenerative myogenesis is essential for proper muscle formation, and although numerous effectors of EMT participate in myogenic differentiation (Kollias and McDermott, 2008; Krauss, 2010), less is known about regulatory factors that coordinate the various facets of this process.

The imprinted *Dlk1-Dio3* locus is the largest known mammalian cluster of noncoding RNAs (ncRNAs), encoding three annotated lncRNAs (*Meg3*, *Rian* and *Mirg*), numerous small nucleolar RNAs (snoRNAs) and over 60 miRNAs co-transcribed from the maternal allele (da Rocha et al., 2008; Benetatos et al., 2013; Dill and Naya, 2018). In recent years, this locus has emerged as a key regulator of cellular processes as diverse as pluripotency and metabolism (Stadtfeld et al., 2010; Liu et al., 2010; Benetatos et al., 2014; Kameswaran et al., 2014; Qian et al., 2016). In muscle, *Dlk1-Dio3* miRNAs function downstream of the MEF2A transcription factor to modulate WNT signaling in differentiation and regeneration, and to regulate mitochondrial activity in satellite cells (Snyder et al., 2013; Wüst et al., 2018; Castel et al., 2018). Dysregulation of *Dlk1-Dio3* ncRNA expression has also been documented in muscular dystrophies and sarcopenia, and in rare congenital growth disorders with pleiotropic organ defects, including hypotonia (Eisenberg et al., 2007; Ogata et al., 2008; Ioannides et al., 2014; Mikovic et al., 2018). Interestingly, a partial deletion of the *Dlk1-Dio3* locus at the 3′end – harboring 22 miRNAs (miR-379/miR-544) – in mice resulted in skeletal muscle hypertrophy (Gao et al., 2015), but not in mice with an additional 17 miRNAs removed from the 3′ end (miR-379/miR-410) (Labialle et al., 2014). Given the vast array of ncRNAs with distinct regulatory activities encoded by this massive and unusually complex locus, much remains to be learned about the individual versus collective function of these ncRNAs.

Recently, the Tabula Muris Consortium performed a large-scale single-cell RNA-sequencing (scRNA-seq) screen of numerous postnatal mouse tissues, including skeletal muscle (Schaum et al., 2018). Although the syncytial nature of skeletal myofibers precluded their analysis by scRNA-seq, this procedure effectively screened multiple mononucleated cells known to be present in the interstitium of this tissue. Analysis of the single-cell muscle transcriptome from this database revealed significantly enriched transcripts of the *Dlk1-Dio3*-encoded lncRNA *Meg3* (also known as *Gtl2*) in satellite cells and mesenchymal stromal cells; these transcripts were largely absent from fibroblasts, endothelial cells and cells of the immune system, including macrophages, B cells and T cells (Schaum et al., 2018). To date, *Meg3* is one of the most comprehensively characterized *Dlk1-Dio3* ncRNAs and has been shown to interact with *Polycomb* repressive complex 2 (PRC2) to regulate chromatin structure in pluripotent embryonic stem cells and neuronal cells (Zhao et al., 2010; Kaneko et al., 2014; Das et al., 2015; Yen et al., 2018). An epigenetic function of *Meg3* has also been reported in human breast and lung cancer cells, where it suppresses TGFβ-related genes to modulate their invasive characteristics (Mondal et al., 2015; Terashima et al., 2017).

Given the enrichment of *Meg3* in muscle satellite cells and its epigenetic function, we hypothesized that *Meg3* regulates cell identity in myoblasts during differentiation and regeneration. To this end, we

Department of Biology, Program in Cell and Molecular Biology, Boston University, Boston, MA 02215, USA.

*Author for correspondence (fnaya@bu.edu)

F.J.N., 0000-0001-5643-2345

Handling Editor: Benoit Bruneau
Received 15 June 2020; Accepted 24 November 2020

Development (2021) 148, dev194027. doi:10.1242/dev.194027

performed *Meg3* knockdown in C2C12 myoblasts and regenerating skeletal muscle to examine for changes in cell identity and mesenchymal character. For both model systems, *Meg3* inhibition upregulated EMT-related genes, resulting in enhanced mesenchymal characteristics and impaired myotube formation, illuminating a key role for *Meg3* muscle cell identity *in vitro* and *in vivo*.

RESULTS

Chronic *Meg3* knockdown in myoblasts impairs myotube formation

To investigate the role of *Meg3* in regulating myoblast identity, we first examined its expression in various muscle-derived cells. Single-cell RNA-sequencing data by *Tabula muris* (Schaum et al., 2018) revealed that *Meg3* expression was restricted to satellite and mesenchymal cells in adult mouse limb muscle, and more enriched than the other two annotated *Dlk1-Dio3* locus lncRNAs: *Rian* and *Mirg* (Fig. 1A). Moreover, *Meg3* was highly upregulated in injury-induced muscle regeneration (Fig. 1B), and enriched in proliferating C2C12 myoblasts, but downregulated upon differentiation (Fig. 1C). Taken together, these data suggest *Meg3* functions in muscle and non-muscle progenitor cells.

Based on the established interaction between *Meg3* and the PRC2 subunit Ezh2 (Zhao et al., 2010; Kaneko et al., 2014; Das et al., 2015), we performed native RNA-immunoprecipitation (RNA-IP) to determine whether *Meg3* interacts with this *Polycomb* complex in proliferating myoblasts. *Meg3* transcripts were enriched 30-fold in Ezh2 immunoprecipitates from C2C12 myoblasts (Fig. 1D) but not in myotubes (Fig. S1A), demonstrating this epigenetic interaction is conserved in muscle progenitor cells.

We next inhibited *Meg3* in C2C12 myoblasts to determine whether *Meg3* is required for muscle differentiation. Given that the *Dlk1-Dio3* ncRNAs are transcribed as a large polycistronic primary RNA (Tierling et al., 2006; Zhou et al., 2010; Luo et al., 2016), processed *Meg3* transcripts were directly targeted with *Meg3*-specific short-hairpin RNA (shRNA) (Mondal et al., 2015) to circumvent unwanted effects on expression of adjoining RNAs in the cluster. Transfected C2C12 myoblasts were subjected to G418 selection, and clonal populations were isolated for differentiation experiments. Both clonal and non-clonal (heterogeneous) populations of myoblasts with stably integrated sh*Meg3* displayed significantly reduced *Meg3* expression compared with sh*LacZ* control myoblasts (Fig. 2A).

To determine the functional consequences of chronic *Meg3* depletion on myoblast differentiation, the ability of C2C12 sh*Meg3* and sh*LacZ* clones to form myotubes was examined. Three days after initiating differentiation sh*LacZ* clones formed numerous multinucleated myotubes with robust expression of myosin heavy chain (MYH4): a differentiation marker expressed in myotubes but not myoblasts (Fig. 2B). In contrast, MYH4-expressing myotubes were largely absent in sh*Meg3* clones, and levels of this protein were dramatically reduced (Fig. 2B,C). Given the difficulty of detecting MYH4 expression in *Meg3*-deficient myoblasts, we immunostained with α-actinin to quantify fusion index, a readout of myotube formation. Fusion was markedly reduced in sh*Meg3* myotubes, with nearly 90% of cells remaining mononucleated, and fewer than 5% containing greater than three nuclei (Fig. 2B, upper graph). In stark contrast, nearly half of all sh*LacZ* control myotubes contained three or more nuclei. Notably, extending the differentiation timeline to day 7 did not improve myotube formation (Fig. S2B).

Supporting the above observations, transcripts for the myogenic regulatory factor genes *Myod1*, myogenin and *Mef2c*, and terminal differentiation marker genes, muscle creatine kinase and skeletal α-actin were significantly reduced in sh*Meg3* myotubes (Fig. 2B, lower graph). These results reinforce the observation that *Meg3* deficiency severely impairs myogenic differentiation.

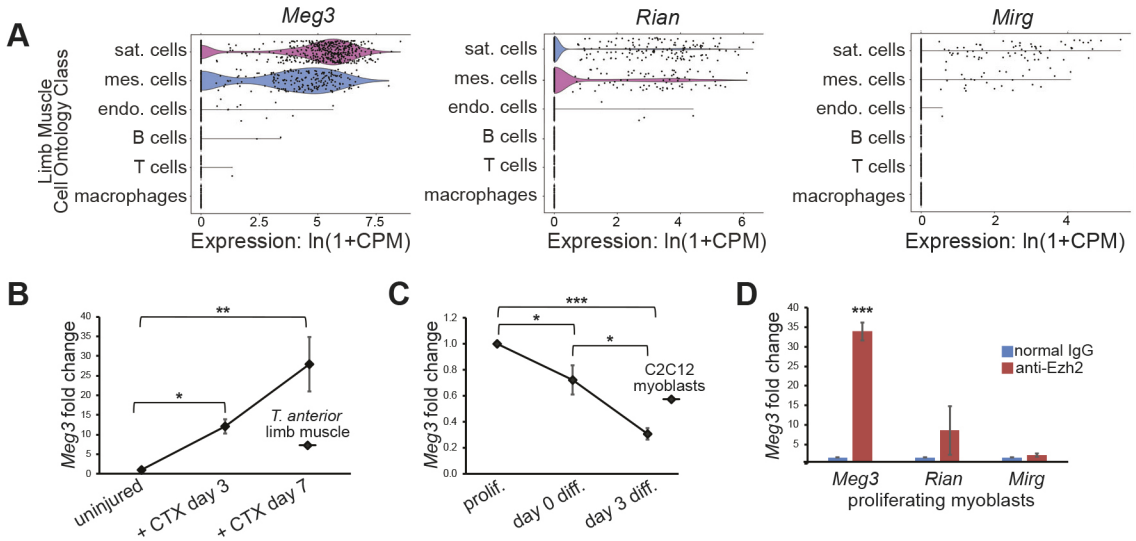

Fig. 1. *Meg3* lncRNA is enriched in muscle progenitors and mesenchymal stromal cells. (A) Violin plots adapted, with permission, from Tabula Muris (Schaum et al., 2018), and are publicly available at https://tabula-muris.ds.czbiohub.org/, depict limb muscle single-cell RNAseq data for *Dlk1-Dio3* megacluster-encoded lncRNAs *Meg3*, *Rian* and *Mirg*. All lncRNAs showed enrichment in satellite (sat.) and mesenchymal (mes.) cell types, with *Meg3* as the most enriched in satellite cells. CPM, counts per million reads mapped. (B) qPCR temporal *Meg3* expression profiling was performed on mouse *tibialis anterior* (TA) muscle tissue harvested from intact muscle (uninjured) and from regenerating muscle on the indicated days after cardiotoxin injection (+CTX). *Meg3* lncRNA transcripts were upregulated following CTX-induced injury, which corresponds with satellite and mesenchymal cell expansion (n=3 mice per time point). (C) qPCR temporal expression profiling of *Meg3* in C2C2 myoblast differentiation. *Meg3* transcripts were most enriched during proliferation (prolif.), and were progressively downregulated during the course of differentiation (n=4). (D) RNA immunoprecipitation (RNA-IP) was performed on subconfluent C2C12 myoblast lysates to examine for *Meg3*-PRC2 interaction. Immunoprecipitated RNA was quantified by qPCR, using supernatant as an internal normalization control. Compared with normal IgG controls, *Meg3* was enriched in anti-Ezh2 immunoprecipitates, whereas *Rian* and *Mirg* were not (n=3 sets of 60 plates).

Development (2021) 148, dev194027. doi:10.1242/dev.194027

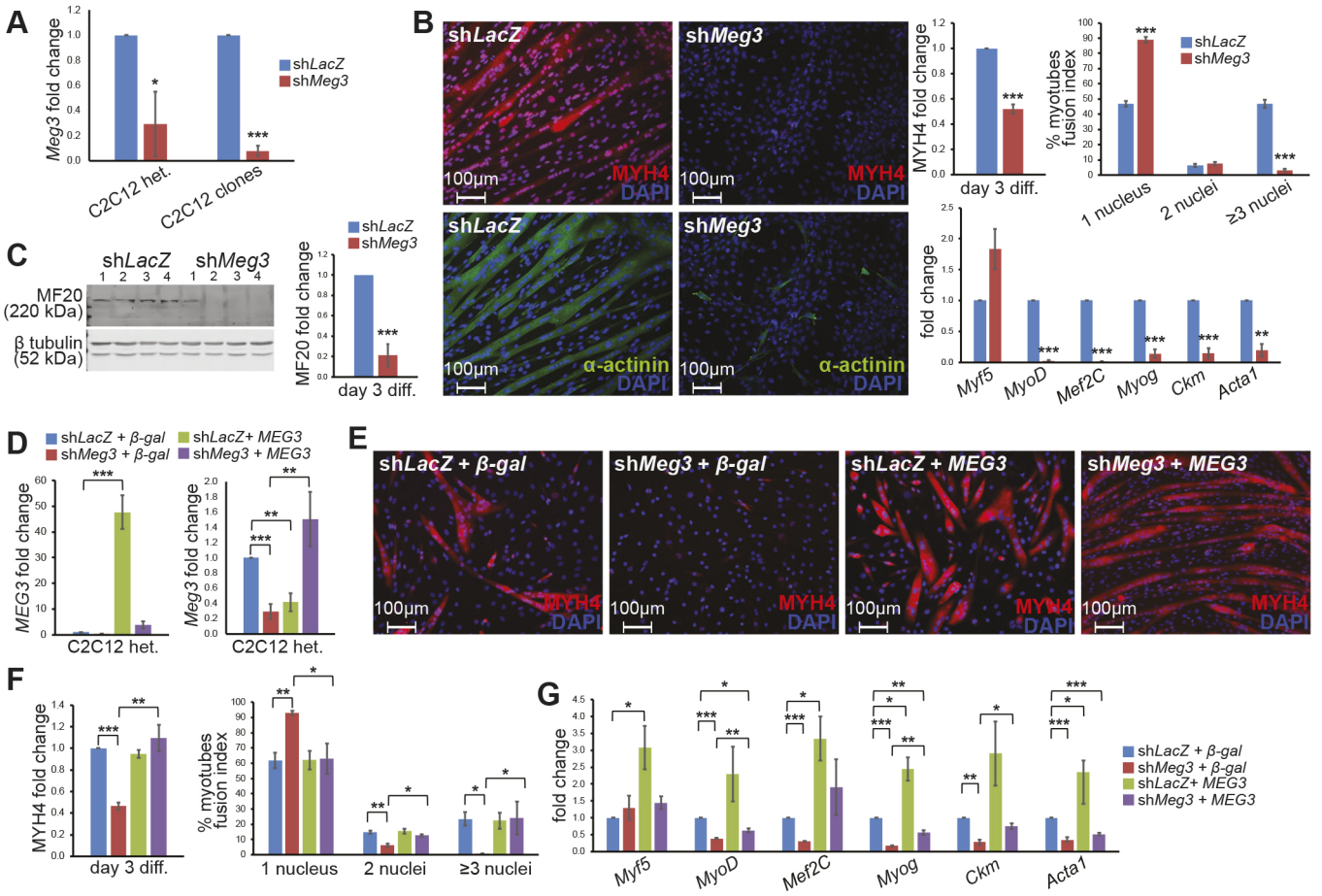

Fig. 2. *Meg3* is required for C2C12 myoblast differentiation. (A) qPCR quantification of *Meg3* transcript levels in heterogeneous cell populations derived from G418 selection (C2C12 het.), and subsequently derived clonal populations (C2C12 clones) indicate that stable shRNA integration resulted in *Meg3* knockdown (n=3). (B) Immunofluorescence quantification of MYH4 indicates markedly reduced expression in sh*Meg3* C2C12 clones. Quantification of nuclei within α-actinin cell boundaries shows a reduced fusion index in sh*Meg3* clones (n=3). qPCR expression profiling indicated unchanged *Myf5* transcript levels, but significant reduction in other myogenic differentiation markers (n=3). (C) Western blot quantification of MF20 signal (normalized to β-tubulin) showed marked reduction specific to sh*Meg3* clones (n=4). (D) qPCR quantification confirmed overexpression of human *MEG3* in sh*LacZ* and sh*Meg3* myoblasts, and restoration of endogenous *Meg3* transcript levels relative to β-galactosidase controls (n=3). (E) Human *MEG3* restored both MYH4 expression and the fusion index in sh*Meg3*, but not sh*LacZ*, myoblasts (n=6, MYH4; n=3, fusion index). (F) qPCR expression profiling of heterogeneous rescue clones revealed an increase in *Mef2c*, *Ckm*, *Myod1* and *Myog* levels in sh*Meg3*+*MEG3* myotubes. *MYH4*, myosin heavy chain 4 (Proteintech antibody); MF20, myosin heavy chain 4 (DHSB antibody); *Myf5*, myogenic factor 5; *Myod1*, myogenic differentiation 1; *Mef2c*, myogenic enhancing factor 2C; *Myog*, myogenin; *Ckm*, muscle creatine kinase; *Acta1*, skeletal muscle actin.

We noted that other RNAs in the locus were downregulated in stable sh*Meg3* clones, presumably due to the complex regulation of this imprinted locus (Fig. S2A) (Das et al., 2015; Luo et al. 2016); therefore, rescue experiments were subsequently performed to demonstrate the specificity of the *Meg3* knockdown phenotype. Because transient overexpression of human *MEG3* failed to rescue differentiation in established sh*Meg3* myoblast lines (Fig. S2C), stable C2C12 myoblasts were generated *de novo* by co-transfection of human *MEG3* or β-galactosidase and either sh*Meg3* or sh*LacZ* expression plasmids. Following G418 selection, expression of human *MEG3* was examined in these co-transfections and found to be increased more than 50-fold in sh*LacZ*+*MEG3* controls, but increased only threefold in sh*Meg3*+*MEG3* myoblasts (Fig. 2D). Comparatively low *MEG3* levels in myoblasts co-transfected with sh*Meg3* were not unexpected, as the sh*Meg3* hairpin targets an evolutionarily conserved *Meg3* sequence shared by mouse, rat and human transcripts. Examination of endogenous *Meg3* expression in sh*Meg3*+*MEG3* myoblasts also revealed that these transcripts were restored to relatively normal levels (Fig. 2D). Stably integrated myoblasts were subsequently induced to differentiate, which resulted in rescue of cytosolic MYH4 expression and fusion index in clones harboring co-integration of sh*Meg3* and human *MEG3* (Fig. 2E,F). In agreement with improved myotube formation, expression of muscle creatine kinase (Ckm) was restored, and Mef2c transcripts were augmented in sh*Meg3* cells by overexpression of human *MEG3*. Moreover, expression of *Myod1* and myogenin (*Myog*) was increased in *MEG3*-treated sh*Meg3* myotubes, although not to the extent observed in sh*LacZ* controls (Fig. 2G). These results clearly demonstrate that *Meg3* functions in myogenic differentiation, and indicates the sh*Meg3*-induced phenotype is not caused by secondary off-target effects.

A differentiation defect in *Meg3*-deficient myoblasts is associated with reduced proliferation, survival and mitochondrial activity

Meg3 is predicted to function as a tumor suppressor via its interaction with p53 (Zhou et al., 2007), leading us to speculate that *Meg3* could regulate proliferation in myoblasts. During expansion

Development (2021) 148, dev194027. doi:10.1242/dev.194027

of sh*Meg3* and sh*LacZ* clones, we noted that *Meg3*-deficient cells grew more slowly than control myoblasts. To determine whether *Meg3* depletion modulates proliferation, we subjected clones to BrdU incorporation assays and found that sh*Meg3* clones exhibit markedly reduced proliferation (Fig. 3A). Moreover, assays for cleaved caspase 3 (Fig. 3B, left) and cell viability (Fig. 3B, right) strongly suggest that *Meg3* depletion also resulted in increased cell death.

Reasoning that impaired myogenic differentiation could be an artifact of low myoblast density, we seeded sh*Meg3* clones at high numbers and subsequently examined their ability to differentiate. However, impaired myogenic differentiation of sh*Meg3* cells persisted even with increased seeding density, as indicated by low cytoplasmic MYH4 expression and fusion index (Fig. 3C). Taken together, these data suggest that *Meg3* is required for normal cell expansion and viability, but failure to form myotubes in *Meg3*-deficient myoblasts is not a consequence of reduced cell-cell contacts.

Because *Dlk1-Dio3* locus expression levels have been shown to correlate with changes in mitochondrial activity in satellite cells (Wüst et al., 2018), we also examined whether *Meg3* depletion affected mitochondria in C2C12 myoblasts. Mutant and control clones were pulsed with MitoTrackerCMXRos and analyzed for mitochondrial mass as myoblasts or myotubes. While Mitotracker Red CMXRos signal increased in response to differentiation conditions within each treatment group, sh*Meg3* clones displayed lower mitochondrial signal when compared with sh*LacZ* clones for early but not late timepoints (Fig. S1B). These data suggest that *Meg3* is required for maintaining normal mitochondrial activity in proliferating, but not differentiating, myoblasts.

Epithelial-mesenchymal transition (EMT) is regulated by *Meg3* and its inhibition alters myoblast identity

To understand the molecular mechanisms of differentiation impairment in sh*Meg3* myoblasts in an unbiased manner, RNA-sequencing (RNA-seq) (Illumina) was performed. Stable *Meg3* knockdown had a profound effect on gene expression, resulting in thousands of transcripts differentially being expressed on differentiation day 3 (Fig. 4A). Despite the expected repressive function of *Meg3* based on its interaction with Ezh2 in C2C12 myoblasts, similar numbers of up- and downregulated transcripts were observed (Fig. 4A). This result is consistent with a satellite cell-specific knockout of Ezh2, which did not result in global derepression of the transcriptome (Juan et al., 2011). The near complete inability to form multinucleated myotubes is reminiscent of defects in myoblast fusion pathways, yet expression of master regulators of myoblast fusion, such as *myomaker* and *myomixer*, was not significantly downregulated (Fig. S3). Curiously, a few fusion

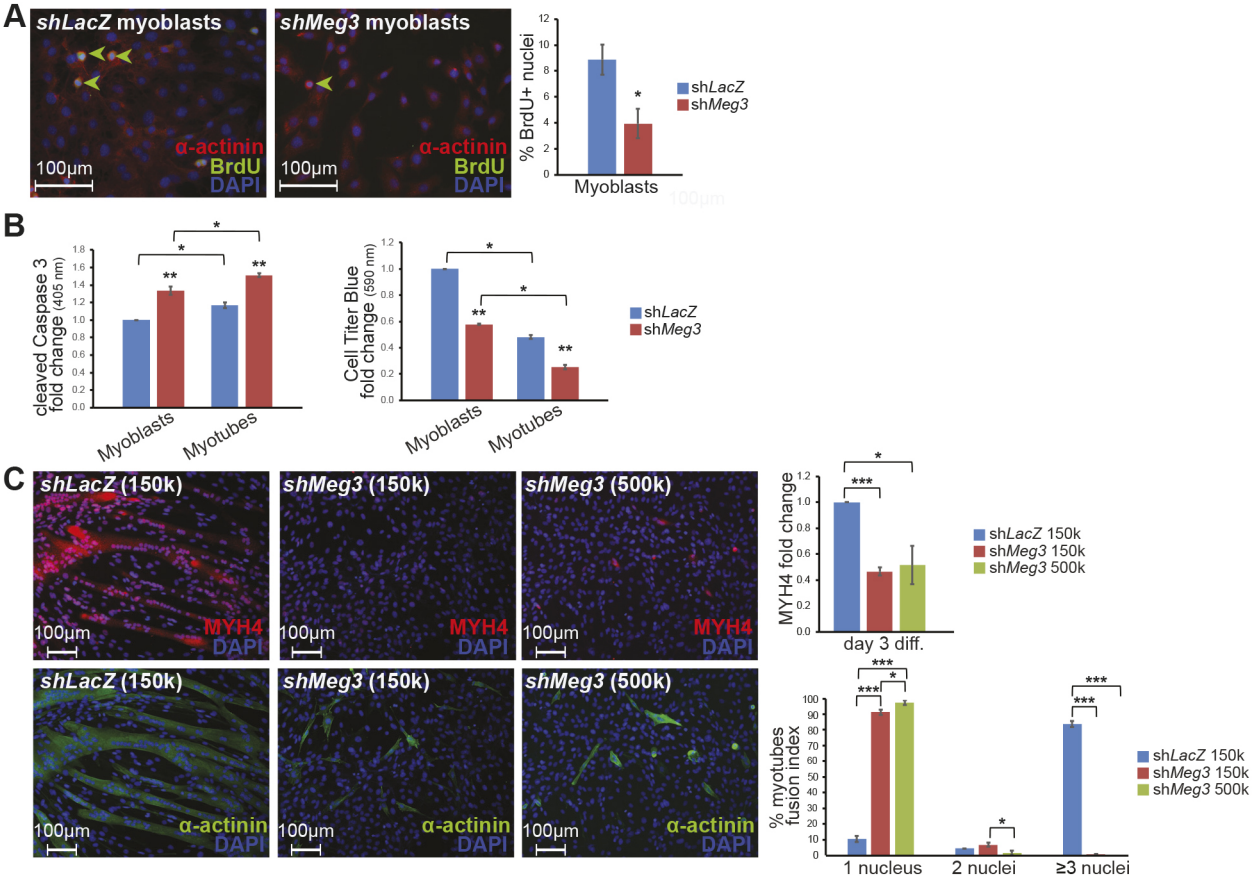

Fig. 3. *Meg3* modulates C2C12 myoblast proliferation and viability. (A) Quantification of BrdU^{+} nuclei (green arrowheads) indicated that sh*Meg3* myoblasts divided at a reduced frequency (n=3). (B) A cleaved caspase 3 assay revealed higher apoptosis in sh*Meg3* myoblasts and myotubes relative to control (left bar graph, n=3). A Cell Titer Blue viability assay indicated reduced viability in sh*Meg3* myoblasts and myotubes relative to control (right bar graph, n=3). (C) Seeding of sh*Meg3* myoblasts at increased densities (500,000 cells per 22 mm^2 coverslip) to increase cell-cell contacts was not sufficient to restore MYH4 expression (top bar graph) or the fusion index (bottom bar graph, n=3).

Development (2021) 148, dev194027. doi:10.1242/dev.194027

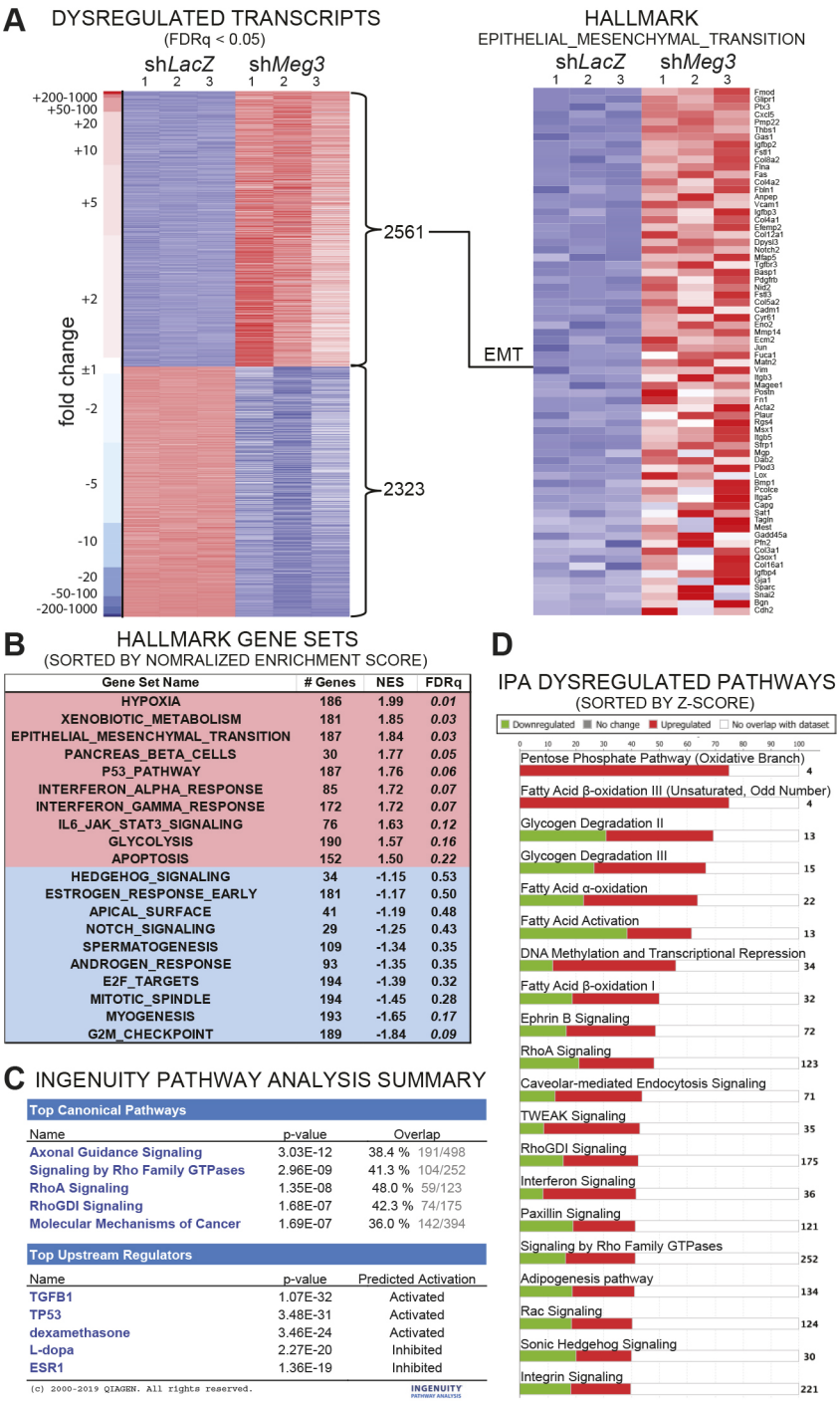

Gene Set Name	# Genes	NES	FDRq
HYPOXIA	186	1.99	*0.01*
XENOBIOTIC_METABOLISM	181	1.85	*0.03*
EPITHELIAL_MESENCHYMAL_TRANSITION	187	1.84	*0.03*
PANCREAS_BETA_CELLS	30	1.77	*0.05*
P53_PATHWAY	187	1.76	*0.06*
INTERFERON_ALPHA_RESPONSE	85	1.72	*0.07*
INTERFERON_GAMMA_RESPONSE	172	1.72	*0.07*
IL6_JAK_STAT3_SIGNALING	76	1.63	*0.12*
GLYCOLYSIS	190	1.57	*0.16*
APOPTOSIS	152	1.50	*0.22*
HEDGEHOG_SIGNALING	34	-1.15	0.53
ESTROGEN_RESPONSE_EARLY	181	-1.17	0.50
APICAL_SURFACE	41	-1.19	0.48
NOTCH_SIGNALING	29	-1.25	0.43
SPERMATOGENESIS	109	-1.34	0.35
ANDROGEN_RESPONSE	93	-1.35	0.35
E2F_TARGETS	194	-1.39	0.32
MITOTIC_SPINDLE	194	-1.45	0.28
MYOGENESIS	193	-1.65	*0.17*
G2M_CHECKPOINT	189	-1.84	*0.09*

Fig. 4. Chronic *Meg3* knockdown in C2C12 myoblasts is associated with activation of EMT and TGFβ. (A) Heatmap of 4884 dysregulated transcripts, with 2561 upregulated (red) and 2323 downregulated (blue). Broad GSEA Hallmark analysis indicated coherent upregulation of well-characterized EMT gene markers. (B) Table conveying the top 10 upregulated (red) and downregulated (blue) Hallmark biological states and cellular processes, as indicated by normalized enrichment score (NES). EMT is among the top three upregulated gene sets. (C) Summary output from Qiagen Ingenuity Pathway Analysis (IPA) software performed with significantly dysregulated transcripts with $P<0.05$. IPA lists TGFβ1 activation as a top upstream regulator, and lists various Rho family pathways among the top canonical pathways. (D) Stacked bar graphs indicate proportions of upregulated (red) and downregulated (green) genes that make up the top 20 dysregulated biological pathways, which include RhoA-related pathways (RhoA signaling, RhoGDI signaling, signaling by Rho family GTPases and Rac signaling).

genes, such as *Kirrel*, *Ehd2* and *Fer1l5*, were found to be upregulated in *Meg3*-deficient myoblasts, suggesting that any effect on fusion would be enhanced rather than impaired.

Gene set enrichment analysis (GSEA) of upregulated transcripts in *Meg3*-deficient myoblasts revealed significant enrichment in metabolism (glycolytic), epithelial-mesenchymal transition (EMT), p53 signaling and apoptosis (Fig. 4B). In contrast, downregulated transcripts were enriched for cell cycle, myogenesis, Notch signaling and apical surface (Fig. 4B). Although the downregulation of myogenesis was entirely consistent with the phenotype of *Meg3*-depleted myoblasts, the GSEA results highlight a broader gene regulatory effect of *Meg3* on cellular processes. To obtain a more focused picture of altered pathways in *Meg3*-deficient myoblasts, we also performed ingenuity pathway analysis (IPA). This analysis revealed a significant enrichment in axonal guidance and Rho signaling, and predicted TGFβ1 as the top upstream regulator of gene expression changes (Fig. 4C,D). Based on the relationship between TGFβ and Rho activity in cytoskeletal remodeling in cell migration (Ungefroren et al., 2018), the integrated GSEA and IPA results indicated that EMT is a key pathway affected by *Meg3* deficiency in C2C12 myoblasts.

We next verified expression levels of genes belonging to EMT, primarily focusing on cellular processes integral to this pathway, such as cell adhesion, migration and cytoskeletal remodeling.

Development (2021) 148, dev194027. doi:10.1242/dev.194027

Initially, expression of cadherins, key mediators of calcium-dependent cell adhesion, was examined for cadherin switching – a well-characterized signature of EMT where E-cadherin becomes downregulated while N-cadherin becomes enriched (Lamouille et al., 2014). As shown in Fig. 5A, expression of mesenchymal *N-cadherin* (*Cdh2*) transcript and protein levels were significantly upregulated in *Meg3* knockdown cells. Although we observed significant downregulation of epithelial *E-cadherin* (*Cdh1*) transcripts, protein was difficult to detect by western blot analysis given the lower sensitivity of this assay and mesenchymal character of myoblasts. These data suggest that *Meg3* knockdown myoblasts have undergone cadherin switching.

Subsequently, expression profiling of selected epithelial and mesenchymal marker genes was examined. Both plakophilin (Pkp1), a cytoskeletal protein that anchors cadherins to intermediate filaments, and *Patj*, a cell-polarity protein crucial for tight-junctions, were downregulated in *Meg3* knockdown cells, while mesenchymal markers fibronectin (*Fn1*), an integrin-binding extracellular matrix glycoprotein, and *Snai2*, a transcriptional repressor of epithelial genes in developmental cell migration and cancer, were both upregulated (Fig. 5B). *Meg3* knockdown did not affect transcript levels of *Twist2*, a bHLH transcription factor associated with carcinogenic EMT, or *Mmp9*, an adhesion-related matrix metallopeptidase (Fig. 5B), nor did it have a significant effect on expression of vimentin, an intermediate filament protein that modulates cell shape and motility (Fig. 5C). Taken together, the bioinformatics and molecular analyses of the sh*Meg3* transcriptome reveal reprogramming of epithelial and mesenchymal gene expression patterns, which strongly suggests activation of EMT and an identity shift towards enhanced mesenchymal character.

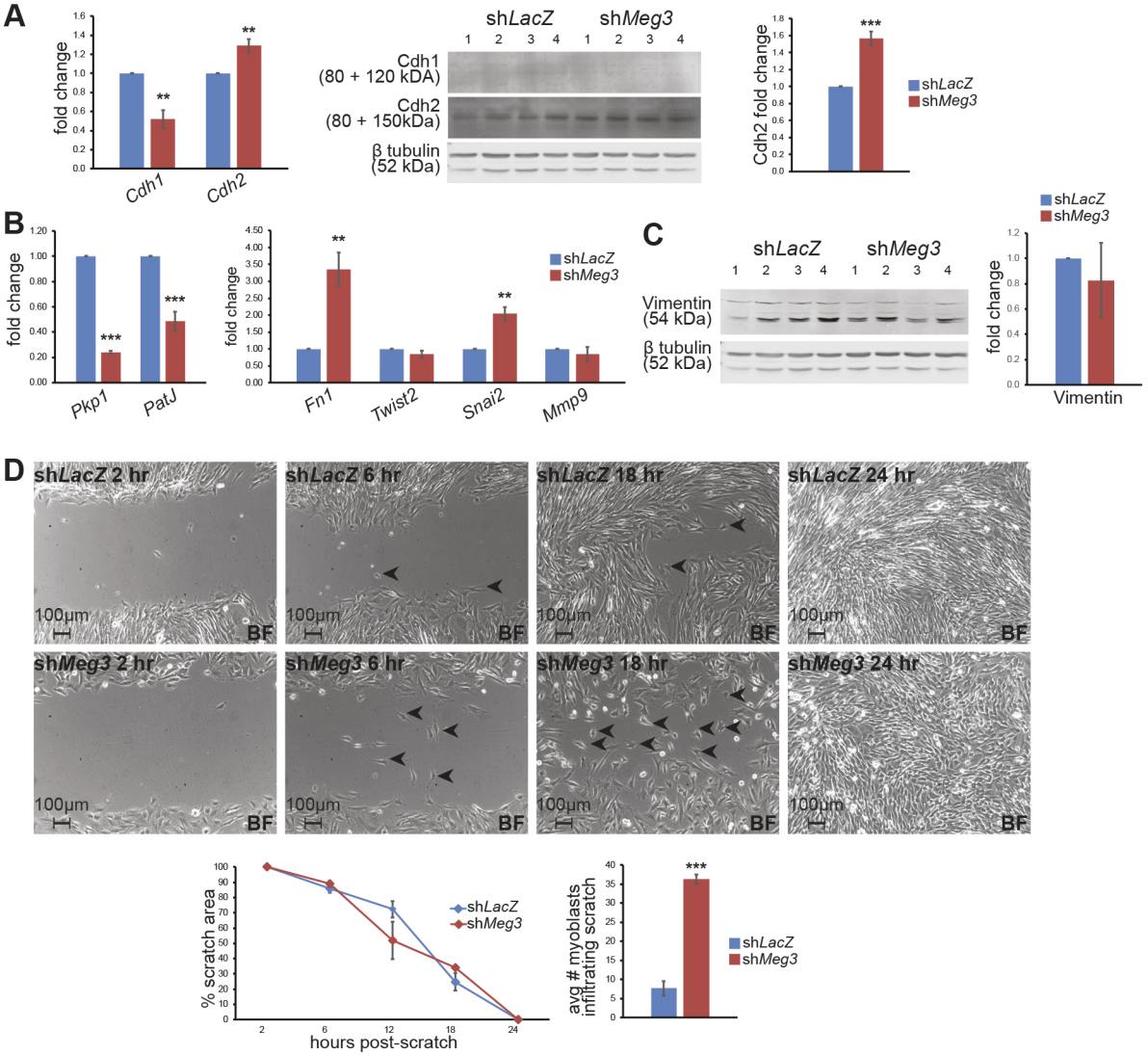

Fig. 5. *Meg3* knockdown enhances the mesenchymal character of C2C12 myoblasts. (A) Cadherin switching was assessed by qPCR (left) and western blot (right) quantification of E-cadherin (Cdh1) and N-cadherin (Cdh2) in day 3 myotubes. *Cdh1* transcripts were significantly downregulated in sh*Meg3* myotubes relative to sh*LacZ* controls (n=3), but Cdh1 protein signal from myotubes lysates was extremely faint (n=4). *Cdh2* transcripts were upregulated (n=3), as was Cdh2 protein (n=4). (B) qPCR expression profiling indicated significant downregulation of epithelial plakophilin and *Patj* transcripts in sh*Meg3* myotubes, with simultaneous upregulation of mesenchymal fibronectin and *Snai2* (n=3). (C) Western blot of vimentin normalized to β-tubulin indicated no change in mesenchymal vimentin (n=4). (D) Scratch-wound assays revealed no detectable change in wound-healing efficiency, as measured by percentage scratch area (n=3). Bright-field (BF) microscopy of wound-healing morphology differed between sh*LacZ* control and sh*Meg3* clones, with a higher proportion of myoblasts invading the scratch territory with fewer than two cell contacts (black arrowheads, n=3).

Development (2021) 148, dev194027. doi:10.1242/dev.194027

Meg3-deficient myoblasts display mesenchymal-like cell adhesion and migration properties

We next sought to investigate cell behavior associated with EMT, such as adhesion and migration in greater detail. To analyze migration, a property enhanced in mesenchymal cells, we performed scratch wound assays to determine whether the observed perturbations in EMT affected this cellular behavior. Measurement of wound closure using the Volkner Wound Healing Tool (ImageJ) indicated no difference in the rate of wound-closure between control and *Meg*3 knockdown C2C12 cells (Fig. 5D). However, the number of infiltrating cells sharing fewer than two borders with neighboring cells was significantly higher in sh*Meg3*-myoblasts, which was most pronounced at the 18 h timepoint (Fig. 5D). By contrast, sh*LacZ* control myoblasts formed sheets reminiscent of collective migration behavior (Campbell and Casanova, 2016). Curiously, we also noted that sh*Meg3* myoblasts required more time to trypsinize during passaging, which may reflect perturbed adhesion properties – and plating these cells on a glass substrate slightly improved fusion of cells with two nuclei, but not three or more nuclei (Fig. S4). These observed changes in migration and adhesion characteristics indicate that activation of EMT in sh*Meg3* myoblasts facilitates mesenchymal behaviors that deviate from normal myoblasts.

Inhibition of the TGFβ signaling pathway restores fusion competence to sh*Meg3* mutant myoblasts

To identify functionally relevant pathways from the vast number of dysregulated transcripts, we examined selected pathways for their ability to modulate the sh*Meg3* differentiation defect. We investigated four dysregulated pathways with documented roles in myogenesis: TGFβ, p53, Notch and sonic hedgehog (Shh). Treatment with constitutively active Notch (Notch-ICD) or Shh (Shh-N) failed to restore differentiation in sh*Meg3* myoblasts (Fig. S5). Treatment with a p53 inhibitor (pifithrin) restored MYH4 levels, but failed to improve fusion (Fig. 6A). In contrast, chemical inhibition of TGFβR1 with LY-2157299 (LY) was sufficient to increase C2C12 sh*Meg3* fusion (cells with three or more nuclei), and increased MYH4 immunofluorescence signal in α-actinin-positive cells (Fig. 6B). Considering TGFβ1 is a potent inhibitor of myogenesis (Kollias and McDermott, 2008), we investigated the effects of this pathway in greater detail. Further analysis revealed the restoration of myosin expression (MF-20) in LY-treated sh*Meg3* myoblasts, and enhancement of myogenic transcripts *Mef2c*, *Myog*, *Ckm* and *Acta1* in sh*Meg3* myotubes (Fig. 6C). As proliferation and survival were also affected by sh*Meg3* treatment, we examined the effect of TGFβ modulation on these processes. Although LY treatment restored proliferation in sh*Meg3* myoblasts (Fig. S6D), it did not restore cell viability (Fig. S6E).

Interestingly, LY treatment resulted in upregulation of both epithelial and mesenchymal EMT markers in sh*LacZ* and sh*Meg3* myotubes, but the extent of dysregulation differed (Fig. S6). In general, sh*Meg3* cells displayed less induction of epithelial, and greater activation of mesenchymal, genes. LY treatment did not downregulate N-cadherin or vimentin protein levels in sh*Meg3* cells, suggesting TGFβ is dispensable for expression of these mesenchymal markers during myotube formation.

The GTPase RhoA functions downstream of TGFβ to remodel the actin cytoskeleton in EMT (Ungefroren et al., 2018), and IPA indicated that this non-canonical TGFβ signaling effector was dysregulated in sh*Meg3* C2C12 cells (Fig. 4C,D). As Rho signaling has been shown to regulate myotube formation (Nishiyama et al., 2004), we treated *Meg3*-deficient myoblasts with the ROCK1/2 inhibitor Y-27632 (Y), a RhoA-dependent protein kinase, and examined MYH4 expression and fusion index. Consistent with the inhibition of TGFβR1, Y-27632 treatment improved myoblast fusion, but did not improve MYH4 expression in sh*Meg3* cells (Fig. 7A).

An additional non-canonical TGFβ effector, p38MAPK, has established functions in promoting EMT and modulating myogenic differentiation of satellite cells (Segalés et al., 2016; Lamouille et al., 2014). We treated sh*Meg3* myoblasts with SB-203580, a specific p38 inhibitor, which resulted in an improved fusion index but, similar to ROCK1/2 inhibition, did not improve MYH4 expression (Fig. 7B). Taken together, these data strongly suggest that RhoA and p38MAPK signaling modulate fusion in myoblasts, and that other effectors downstream of TGFβ likely regulate MYH4 expression.

Examination of the canonical TGFβ pathway revealed that Smad3 inhibition was not sufficient to restore differentiation, suggesting that aberrant non-canonical signaling drives the fusion defect observed in sh*Meg3* cells (Fig. 7C). TGFβ is a negative regulator of muscle growth and BMP signaling is thought to work antagonistically to produce pro-myogenic effects, including muscle mass enhancement (Sartori et al., 2013). However, we found that sh*Meg3* myoblasts were largely unresponsive to BMP4 treatment, which was not sufficient to improve MYH4 expression or fusion (Fig. S6F). These findings indicate that TGFβ-mediated suppression of myogenic differentiation likely overrides BMP4-mediated myogenic enhancement, and reinforces the notion that abnormal TGFβ activation is a primary bottleneck for sh*Meg3* myogenic differentiation.

To explore the connection between TGFβ and EMT we examined expression of Snai2, a major transcriptional regulator of EMT, in sh*Meg3* myoblasts treated with LY. As shown in Fig. 8A,B, Snai2 was enriched in sh*Meg3* myoblasts, and enrichment was dependent on TGFβ. Additionally, treatment with siSnai2 improved fusion in sh*Meg3* myoblasts (Fig. 8C). Thus, *Meg3* is required to modulate TGFβ-dependent Snai2 activity, which facilitates myogenic fusion.

Meg3 regulates PRC2 and histone methylation in myoblasts at TGFβ loci

To define the molecular mechanisms underlying the *Meg3* knockdown phenotype, we reasoned that depletion of Meg3 would result in PRC2-mediated changes in the epigenetic landscape of sh*Meg3* myotubes. To this end, we performed chromatin immunoprecipitation (ChIP) for the PRC2 catalytic component Ezh2, as well as its signature epigenetic mark H3K27me3. qPCR was performed to examine for sh*Meg3*-dependent epigenetic changes in 57 loci: 25 distal enhancers with homology to human loci reported by Mondal et al. (Table S2) and 32 transcription start site (TSS) loci with documented H3K27me3 enrichment in mouse muscle progenitor cells (Table S3).

Ezh2 yielded generally low percentage of input for all loci surveyed (Fig. S7B), which correlated with cytoplasmic export and reduced expression of Ezh2 at day 3 of differentiation (Fig. S7A). In contrast, H3K27me3 was detectable over IgG negative control (Fig. S7C), and several TGFβ loci were subsequently examined for repressive H3K27me3 enrichment (Fig. 9A). Notably, reduced H3K27me3 enrichment was observed at the TSS of TGFβ signal ligands TGFβ1 and TGFβ2, as well as the distal enhancer of the canonical signaling component Smad2, in

Development (2021) 148, dev194027. doi:10.1242/dev.194027

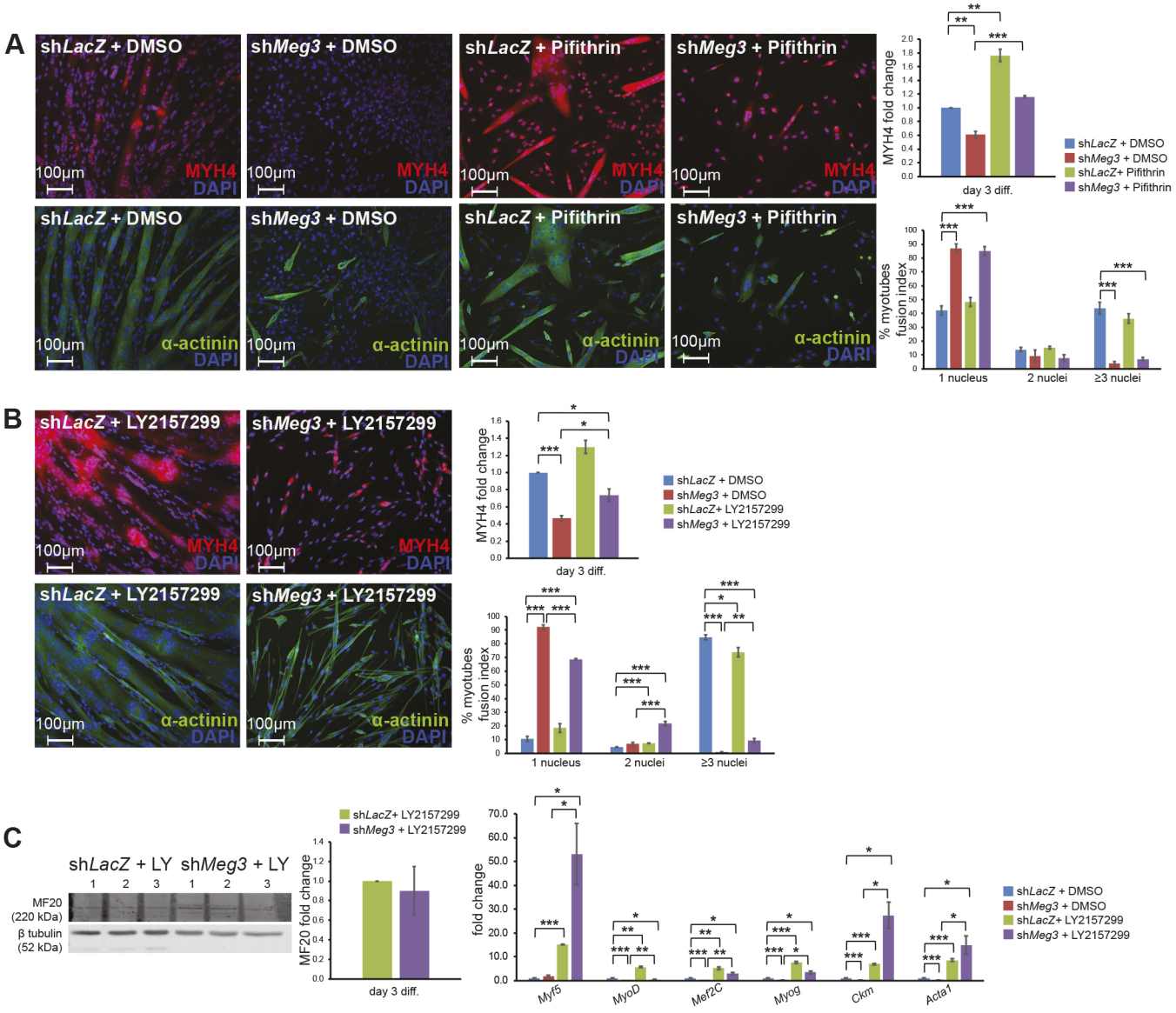

Fig. 6. Pharmacological inhibition of TGFβR1 restores fusion competence and myogenic differentiation in *Meg3*-deficient myoblasts. (A) Following incubation with 30 µM p53 inhibitor Pifithrin-α hydrobromide (Pifithrin), myoblasts were induced to differentiate and examined for MYH4 expression and fusion index. MYH4 was restored to sh*LacZ* control levels. Although multinucleated myotubes were occasionally observed, these improvements were not abundant enough for statistical significance (*n*=3). (B) Following incubation with 10 µM TGFβR1 inhibitor LY2157299 (LY), myoblasts were induced to differentiate and examined for MYH4 expression and fusion index. LY-treated sh*Meg3* myotubes adopted an elongated morphology, and displayed increased MYH4, decreased myotubes with one nuclei and increased myotubes with two or more nuclei relative to untreated sh*Meg3* controls (*n*=3). (C) Western blot for MF20 indicated that LY treatment restored myosin heavy chain 4 expression to sh*Meg3* myotubes (*n*=3). qPCR expression profiling of LY-treated myotubes indicates significant upregulation of all myogenic markers surveyed (*Myf5*, *Myod1*, *Mef2c*, *Myog*, *Ckm* and *Acta1*) relative to untreated sh*LacZ* myotubes (*n*=3).

sh*Meg3* myotubes. Moreover, H3K27me3 was enriched at the TSS of Ltbp2 and, to a lesser extent, Ltbp4, which are required for restriction of TGFβ ligand bioavailability. Finally, the distal enhancer of the BMP4 signaling antagonist Smad6, which competes with Smad4 for Smad1/5/8 binding, displayed markedly reduced H3K27me3 enrichment, and feasibly could contribute to the lack of BMP4 responsiveness observed in Fig. S6F. Taken together, these epigenetic perturbations likely reinforce the aberrant TGFβ signaling observed in sh*Meg3* cells, which prompted further investigation of Ezh2-mediated perturbations.

Interestingly, H3K27me3 was enriched in the nuclei of sh*Meg3* C2C12 myoblasts and myotubes (Fig. 9B, top panel). As expected, treatment of proliferating C2C12 myoblasts with Unc1999, a chemical inhibitor of Ezh2 activity, globally reduced H3K27me3 levels in myoblasts (Fig. 9B, bottom panel), and differentiation of Unc1999-treated sh*Meg3* cells resulted in both MYH4 and fusion improvements (Fig. 9C). Importantly, the TGFβ-dependent EMT marker Snai2 was downregulated only with Unc1999 treatment in sh*Meg3* myotubes, suggesting Ezh2 activity is altered to promote TGFβ-dependent Snai2 expression in sh*Meg3* cells (Fig. 9C, bottom panel). These findings, coupled with data previously shown in Fig. 1D, strongly suggest that *Meg3* is required for maintenance of a myogenesis-competent epigenetic state in proliferating myoblasts, in part via H3K27me3-dependent regulation of TGFβ signaling.

Development (2021) 148, dev194027. doi:10.1242/dev.194027

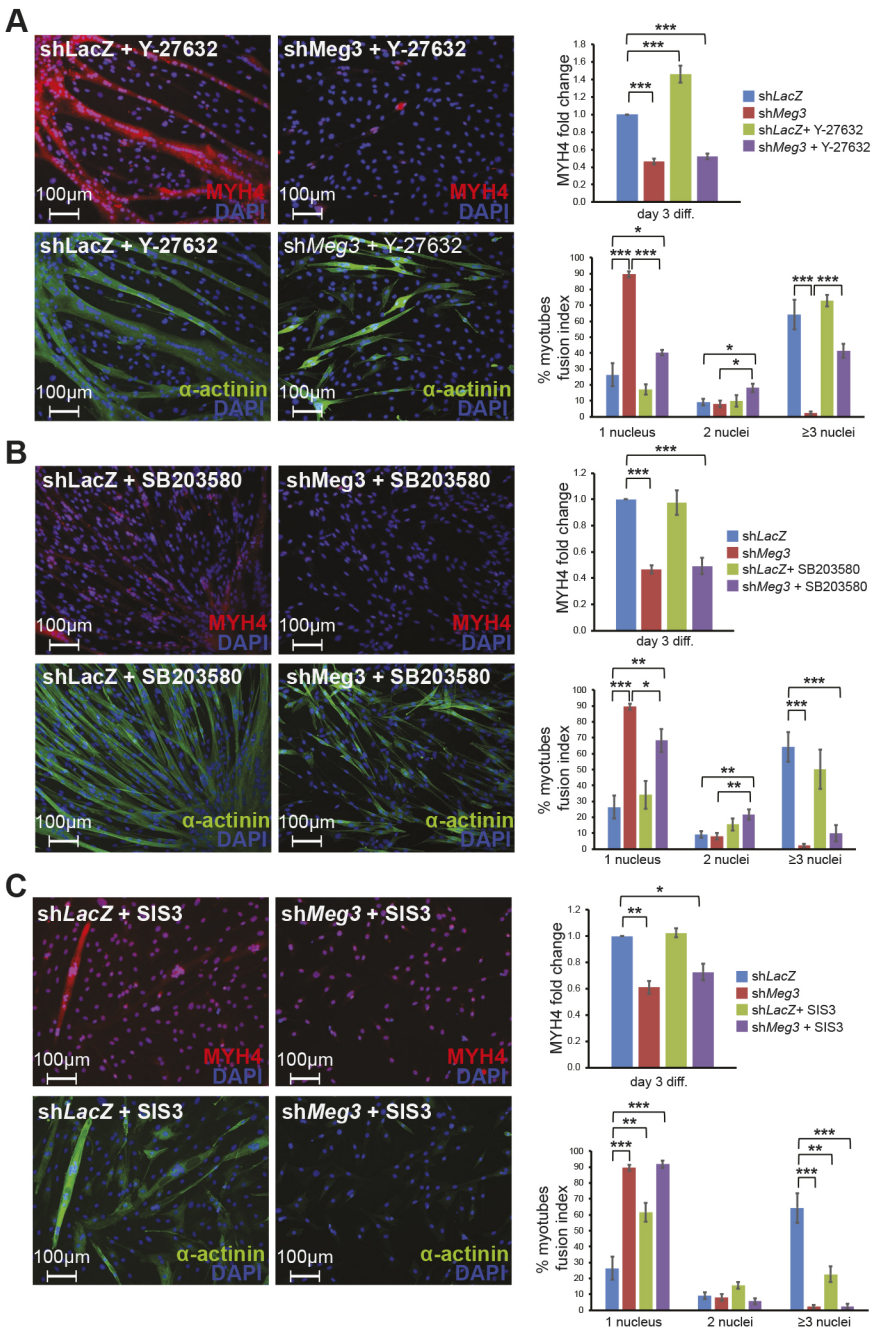

Fig. 7. Pharmacological inhibition of Rho GTPase and p38 MAPK restores myotube formation. (A) Following incubation with 40 μM ROCK1/2 inhibitor (Y-27632), myoblasts were induced to differentiate and examined for MYH4 expression and fusion index. Y-27632-treated sh*Meg3* myotubes adopted an elongated morphology, and fusion quantification indicated decreased myotubes with one nuclei, and increased myotubes with two or more nuclei relative to sh*Meg3* control (n=3). While MYH4 expression was enhanced in sh*LacZ*+Y-27631 myotubes, MYH4 levels remained unchanged with Y-27632 treatment in sh*Meg3* cells (n=3). (B) Following incubation with 10 μM p38 inhibitor (SB203580), myoblasts were induced to differentiate and examined for MYH4 expression and fusion index. SB203580-treated sh*Meg3* myotubes adopted an elongated spindle-like morphology, and fusion quantification indicated decreased myotubes with one nuclei, and increased myotubes with two or more nuclei relative to sh*Meg3* control (n=3). MYH4 expression was unaffected by SB203580 treatment (n=3). (C) Following incubation with 5 μM Smad3 inhibitor (SIS3), myoblasts were induced to differentiate. MYH4 expression and fusion index were unaffected by SIS3 treatment in sh*Meg3* myotubes (n=3).

Meg3 knockdown in injured skeletal muscle severely disrupts the normal regenerative response

Based on the enrichment of *Meg3* transcripts in satellite cells and mesenchymal stromal cells, we reasoned that this lncRNA functions in the injured skeletal muscle microenvironment and regulates the identity of these progenitor cell types for proper myofiber regeneration. To circumvent the perinatal lethality of *Meg3* knockout mice (Zhou et al., 2010) and other aforementioned effects relating to the polycistron, we used shRNA to knock down *Meg3* in adult skeletal muscle. To this end, the *tibialis anterior* (TA) muscles of mice were injured by cardiotoxin (CTX) co-injected with either sh*Meg3*- or sh*LacZ*-specific adenovirus. Regenerating TA muscles were harvested for expression analysis, and significant downregulation of *Meg3* was confirmed in muscle at 3 days post-injury (Fig. 10A and Fig. S8B).

Whole-mounts of regenerating TA muscle treated with sh*Meg3* adenovirus exhibited more pronounced necrotic regions at days 3 and 7 post-injury that diminished by day 14 (Fig. 10B). Regenerating sh*Meg3* muscle sections also harbored regions with intense basophilic stain at a higher frequency than observed in sh*LacZ* control TA muscle (Fig. 10C). To evaluate for changes in cross-sectional area (CSA), an indicator of myoblast fusion, injured TA muscle sections were analyzed by laminin immunofluorescence. While *Meg3* levels increased in injured sh*Meg3* TA muscle by 7 days post-injury (Fig. S8C), the CSA of sh*Meg3* myofibers was not only significantly reduced in sh*Meg3*-treated TA muscle at day 3, but also at day 7 and 14 post-injury (Fig. 10D and Fig. S8A). Notably, overexpression of MEG3 did not significantly affect muscle regeneration (Fig. S8D,E). These findings suggest that inhibition of *Meg3* at the onset of injury, when muscle and non-

Development (2021) 148, dev194027. doi:10.1242/dev.194027

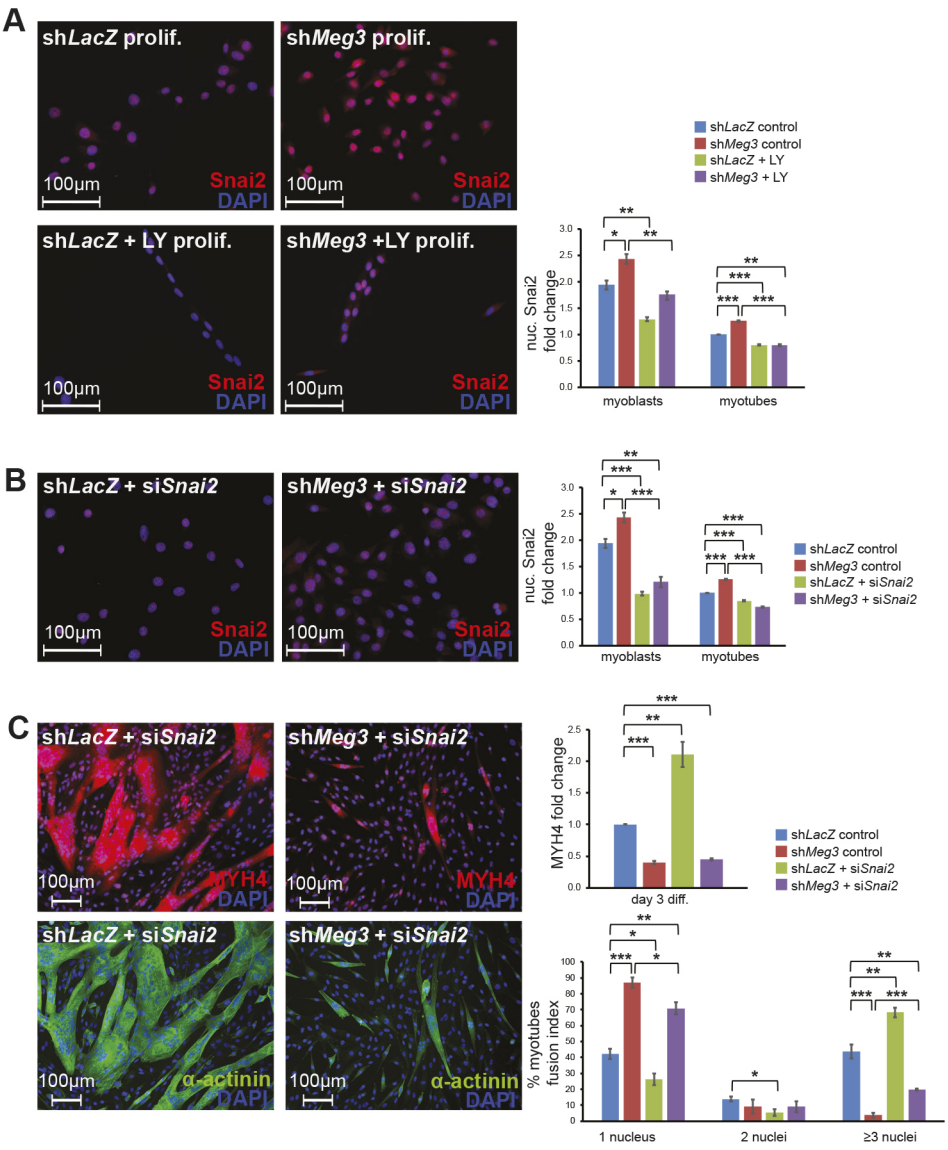

Fig. 8. TGFβ-dependent Snai2 is upregulated in *Meg3* knockdown.
(A) Subconfluent C2C12 myoblasts and day 3 differentiated myotubes were examined for Snai2 nuclear intensity, with or without 10 µM TGFβR1 inhibitor LY2157299 (LY) treatment. Snai2 was significantly enriched in no-treatment control sh*Meg3* myoblasts for both timepoints, and LY treatment significantly downregulated Snai2 nuclear intensity (*n*=3). (B) Treatment with 500 ng siRNA targeting *Snai2* (si*Snai2*) resulted in significant Snai2 protein, as measured by immunofluorescence (*n*=3). (C) Differentiation of si*Snai2*-treated cells revealed an enhanced fusion index, and while MYH4 was enhanced in sh*LacZ*+si*Snai2* myotubes relative to sh*LacZ* controls, no change in MYH4 was detected in sh*Meg3* cells treated with si*Snai2* (*n*=3).

muscle precursors are activated, had long-lasting detrimental effects on muscle regeneration.

Increased proliferation of mesenchymal stromal, but not satellite, cells in injured sh*Meg3* muscle

Given that *Meg3* has well-documented roles modulating proliferation in a variety of cell types, and the proliferation defect observed in sh*Meg*3 C2C12 myoblasts, we considered the possibility that *Meg3* modulates this process in regenerating muscle. To this end, proliferation in muscle stem cells was examined by immunofluorescence using Ki67, a marker of actively cycling cells, and Pax7, a muscle stem cell (satellite cell) marker. Quantification of Ki67 revealed a significant increase in protein signal, but this elevated expression was independent of satellite cells (Fig. 10E, lower left bar graph). Consistent with this observation, there was a significant increase in the number of Ki67+/Pax7−, but not Ki67+/Pax7+ mononucleated cells (Fig. 10E, lower left graph). Moreover, the total number of Pax7+ cells did not change in regenerating sh*Meg*3-treated muscle at day 7 post-injury (Fig. 10E, lower left). These data reveal that elevated cell cycle activity in regenerating *Meg3*-deficient muscle is attributable to a non-satellite cell population.

To define this non-satellite cell population, we subsequently examined expression of PDGFRα, a marker for limb muscle mesenchymal stromal cells – also known as fibroadipogenic progenitors (FAPs) (Joe et al., 2010) – that express *Meg3* lncRNA (Fig. 1A). As shown in Fig. 10F, a marked increase in expression and number of PDGFRα+ cells was observed in sh*Meg*3 relative to sh*lacZ* control muscle. Consistent with these findings, Sirius Red stain revealed increased fibrosis at day 14+CTX (Fig. 12E). These data indicate that *Meg3* knockdown stimulates mesenchymal stromal cell expansion rather than changes in the abundance of satellite cells, and suggest that reduced myofiber CSA is not a consequence of reduced satellite cell number, but rather of defects in satellite cells unrelated to proliferation.

Enhanced mesenchymal-like properties in *Meg3*-depleted regenerating muscle

To precisely define the molecular mechanisms of impaired myofiber formation in *Meg3*-deficient regenerating muscle, RNA-seq was performed on TA muscle tissue 7 days post-injury. The dysregulated transcriptome of injured sh*Meg3*-treated muscle revealed significant enrichment of genes involved in EMT (Hallmark) and TGFβ signaling (Hallmark and IPA),

Development (2021) 148, dev194027. doi:10.1242/dev.194027

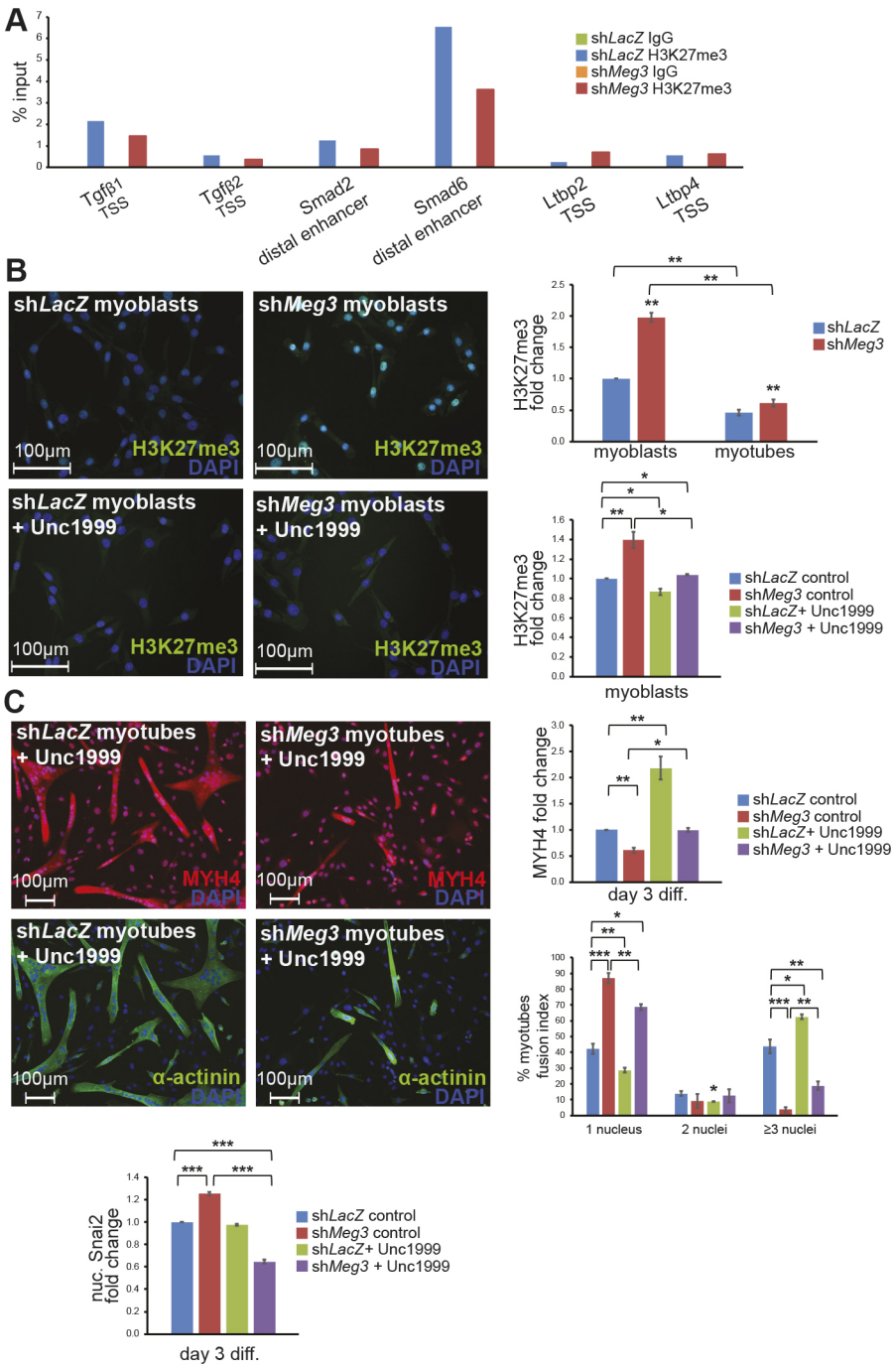

Fig. 9. *Meg3* knockdown dysregulates Ezh2 activity on TGFβ loci. (A) Analysis of day 3 differentiation myotubes revealed modulations of H3K27me3 enrichment in the transcription start sites (TSSs) and distal enhancers for several TGFβ-related loci (*n*=1 set of 30 pooled plates). (B) Immunofluorescent quantification of H3K27me3 revealed enriched H3K27me3 signal in sh*Meg3* myoblasts and day 3 myotubes, relative to the sh*LacZ* controls. Treatment of C2C12 clones with 2 μM Ezh2 inhibitor (Unc1999) reduced H3K27me3 signal (*n*=3). (C) Differentiation of Unc1999-treated myoblasts revealed that sh*Meg3* MYH4 signal and fusion are both improved with Ezh2 inhibition (*n*=3). Furthermore, immunofluorescent quantification of nuclear Snai2 at this timepoint revealed that Ezh2 treatment only downregulated Snai2 in sh*Meg3* clones (*n*=3).

similar to that observed in *Meg3*-deficient C2C12 myoblasts (Fig. 11A-D).

Based on these results, we examined for cadherin switching, and confirmed that N-cadherin transcripts (*Cdh2*) were upregulated in sh*Meg3* muscle 7 days post-injury (Fig. 12A, left graph). In contrast, E-cadherin transcripts (*Cdh1*) were unchanged, and protein signal was undetectable (data not shown). Detailed examination of N-cadherin protein at the cellular level revealed that its expression was largely restricted to Pax7+ cells. Although N-cadherin intensity per satellite cell was unchanged (Fig. 12A, right graph), the percentage of satellite cells expressing N-cadherin was significantly increased in *Meg3*-deficient muscle (Fig. 12A, middle graph). These data indicate an enrichment of mesenchymal adhesion properties in satellite cells in regenerating sh*Meg3*-treated muscle, even in the absence of a bona fide switch.

To further analyze EMT in regenerating muscle, expression of additional epithelial and mesenchymal markers was examined. Epithelial marker genes plakophilin and *Patj* were unaffected by sh*Meg3* treatment, but mesenchymal markers fibronectin and *Snai2* were significantly increased (Fig. 12B). To delve deeper into the increased mesenchymal marker expression observed in sh*Meg3* muscle, we analyzed protein localization of the EMT transcription factor Snai2, which is regulated, in part, through nucleo-cytoplasmic shuttling (Lamouille et al., 2014). Snai2 was detected in satellite cells, in Pax7-negative mononucleated cells and in regenerating myofibers, and the proportions of these Snai2+ cells

Development (2021) 148, dev194027. doi:10.1242/dev.194027

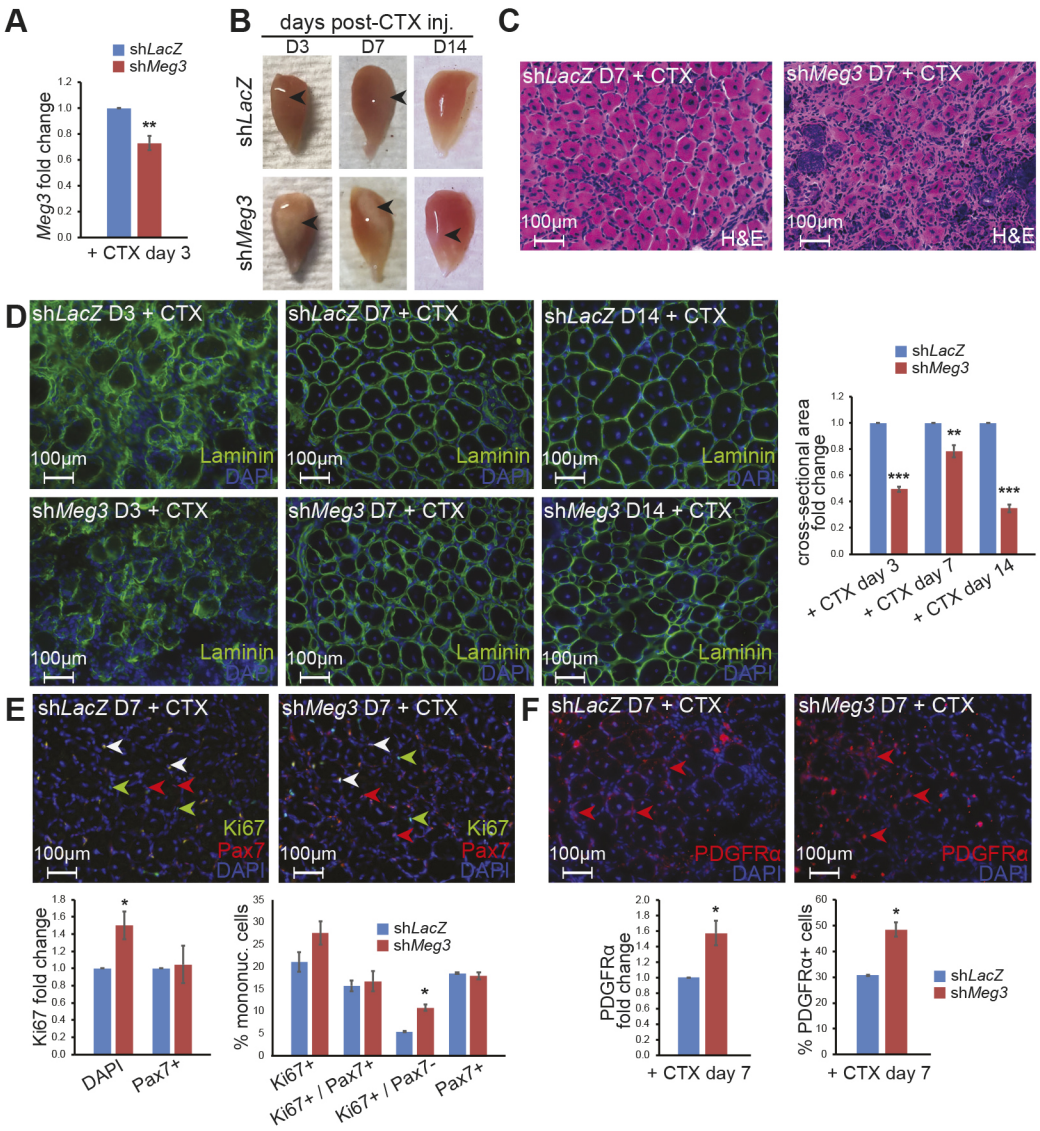

Fig. 10. *Meg3* knockdown impairs injury-induced skeletal muscle regeneration. (A) qPCR expression profiling indicated reduced *Meg3* expression in TA muscles co-injected with sh*Meg3* adenovirus (n=3). (B) Whole-mount morphology of regenerating muscles co-injected with adeno-sh*LacZ* (top) or adeno-sh*Meg3*. (C) Hematoxylin and Eosin staining of muscle sections. (D) Cross-sectional area (CSA) of laminin-ensheathed regenerating myofibers was measured for days 3, 7 and 14 post-CTX injury. sh*Meg3* muscle displayed reduced CSA for all time points surveyed. (E) Immunofluorescence quantification indicated sh*Meg3* TA sections harbor increased Ki67 signal (left graph). Co-staining for Pax7 indicated no change in satellite-cell specific Ki67 signal (right graph) and no change in satellite cell abundance (white and red arrowheads). Marker quantification revealed an increase in proliferating cells lacking Pax7 co-stain (green arrowheads). (F) Immunofluorescence quantification indicated an increase in PDGFR signal, as well as increased abundance of PDGFRα$^+$ cells (red arrowheads).

did not change with sh*Meg3* treatment (Fig. 12C, left graph). However, although all Snai2$^+$ cells had increased cytoplasmic Snai2 (Fig. 12C, right graph, DAPI), only satellite cells displayed significantly more intense nuclear Snai2 signal compared with sh*LacZ* controls (Fig. 12C, right graph, Pax7). Although multiple cell types displayed aberrant accumulation of Snai2 in the cytoplasm, its increased nuclear localization in satellite cells is consistent with upregulation of other mesenchymal genes, and strongly suggests an increased ability to activate EMT in these progenitors.

Vimentin expression was analyzed and detected in numerous mononucleated cells, including a subset of satellite cells, in the regenerating muscle microenvironment. Although the overall percentage of vimentin$^+$ mononucleated cells was increased, this net increase can be attributed to Pax7$^-$ cells, as vimentin$^+$ satellite cells were reduced (Fig. 12D, left graph). Interestingly, with the exception of satellite cells, there was less vimentin expressed per cell in sh*Meg3* muscle, reflecting an overall reduction in its synthesis (Fig. 12D, right graph). Analysis of vimentin at a later timepoint revealed more pronounced abundance of vimentin$^+$ populations in sh*Meg3* muscle (Fig. 12D, left panel). Interestingly, vimentin levels were enriched in Pax7$^-$ cells at this timepoint, suggesting increased mesenchymal character in these cells (Fig. 12D, right panel). Taken together, *Meg3* inhibition predominantly impacted vimentin expression in cells that are not of satellite cell origin.

Overall, these data reveal that knockdown of *Meg3* in the context of cardiotoxin-induced muscle injury dramatically remodeled the

Development (2021) 148, dev194027. doi:10.1242/dev.194027

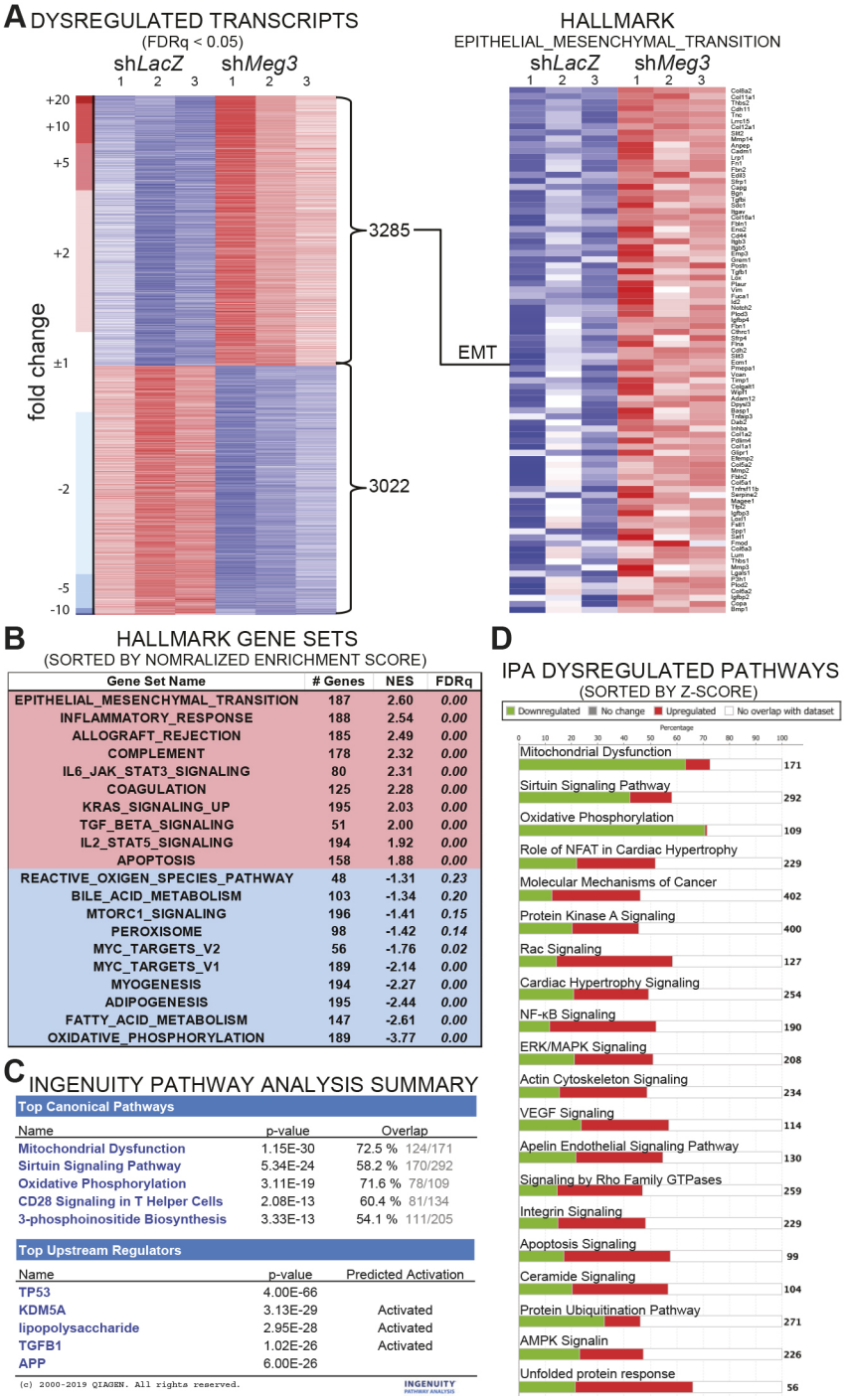

Fig. 11. EMT and TGFβ signaling are among the top dysregulated pathways in regenerating *Meg3* knockdown muscle. (A) Heatmap of 6307 dysregulated transcripts, with 3285 upregulated (red) and 3022 downregulated (blue). Broad GSEA Hallmark analysis indicated coherent upregulation of well-characterized EMT gene markers. (B) Table conveying the top 10 upregulated (red) and downregulated (blue) Hallmark biological states and cellular processes, as indicated by normalized enrichment score (NES). EMT was the top upregulated gene set. (C) Summary output from Qiagen Ingenuity Pathway Analysis (IPA) software performed with significantly dysregulated transcripts (P<0.05). IPA lists TGFβ1 among the top upstream regulators, and lists various metabolic pathways among the top canonical pathways. (D) Stacked bar graphs indicate proportions of upregulated (red) and downregulated (green) genes that make up the top 20 dysregulated biological pathways, which include metabolic pathways (mitochondrial dysfunction, sirtuin signaling, oxidative phosphorylation and protein kinase A signaling), RhoA-related pathways (Rac signaling and signaling by Rho family GTPases) and EMT-related pathways (molecular mechanisms of cancer, ERK/MAPK signaling, actin cytoskeleton signaling and integrin signaling).

regenerating tissue microenvironment by triggering aberrant EMT activation in satellite cells and – to a lesser extent – non-satellite cells.

DISCUSSION

Our findings reveal a key role for the lncRNA *Meg3* in myoblast plasticity and highlight the importance of proper regulation of EMT and TGFβ signaling for myogenic differentiation. Chronic depletion of *Meg3* in C2C12 myoblasts resulted in an enhanced mesenchymal cell state, marked by imbalance of epithelial and mesenchymal genes, which diminished growth and differentiation. Moreover, *Meg3* inhibition in skeletal muscle injury severely impaired myofiber formation, increased mesenchymal gene expression in satellite cells and resulted in abnormal mesenchymal stromal cell expansion, radically altering the cellular composition in the regenerating microenvironment. In both models, transcriptomic profiling indicated that *Meg3* regulates EMT through repression of TGFβ signaling, and inhibition of TGFβR1 – or its downstream effectors RhoA, p38MAPK or Snai2 – was sufficient to restore aspects of myogenic fusion and differentiation *in vitro*.

Like many imprinted genes, expression of the *Dlk1-Dio3* locus correlates with changes in cell state (Stadtfeld et al., 2010; Liu et al., 2010; Haga and Phinney, 2012; Qian et al., 2016), and *Meg3* has emerged as a major driver of these adaptations. *Meg3* has been

Development (2021) 148, dev194027. doi:10.1242/dev.194027

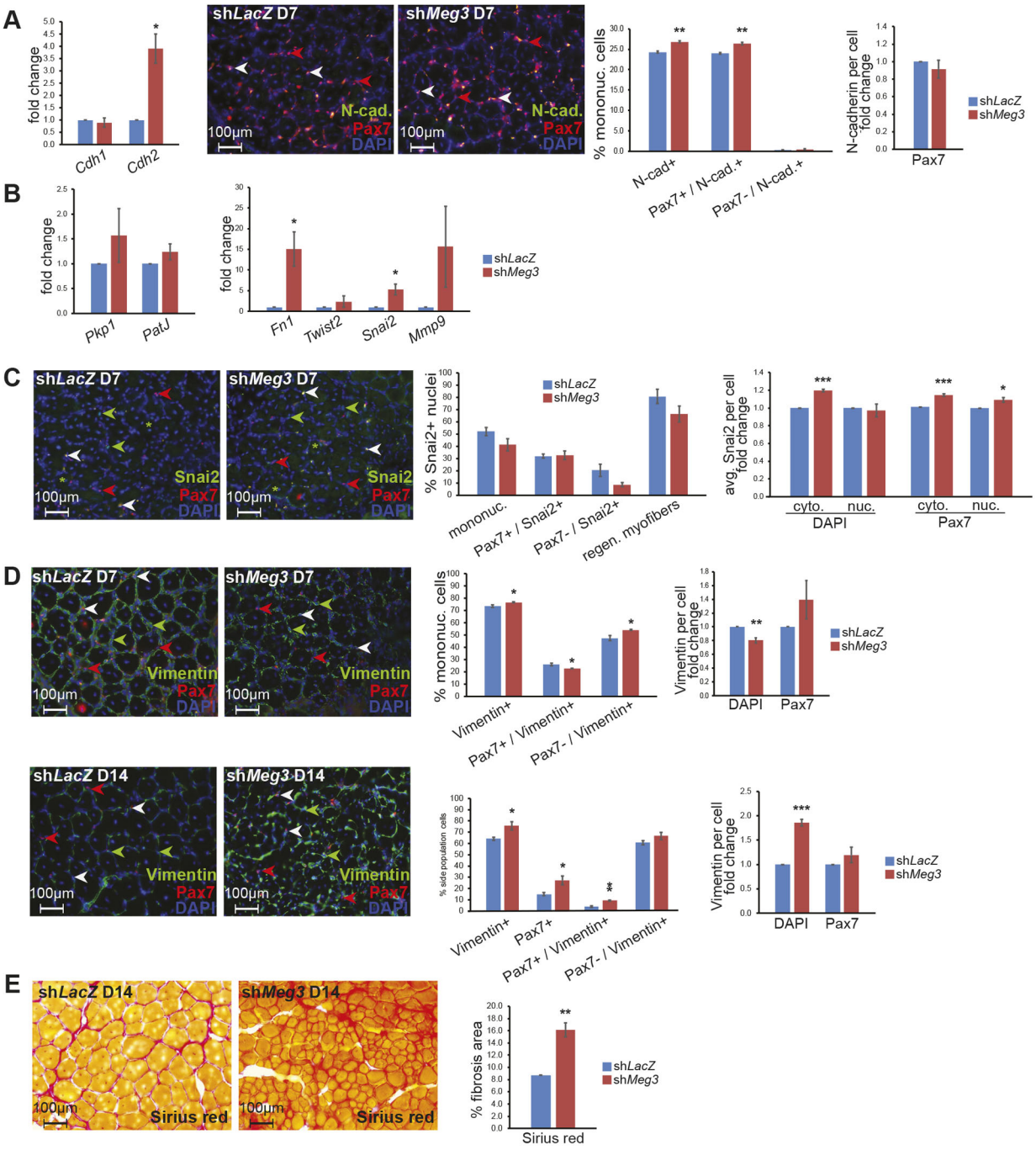

Fig. 12. Enhanced mesenchymal character in *Meg3* knockdown regenerating muscle microenvironment. (A) Expression profiling by qPCR indicated no change in E-cadherin (*Cdh1*), whereas day 7 sh*Meg3* muscle was enriched for N-cadherin (*Cdh2*) transcripts (n=3). Immunofluorescence revealed that, although numerous satellite cells were not N-cad$^+$ (red arrowheads), N-cad signal was largely restricted to Pax7$^+$ satellite cells in regenerating muscle (white arrowheads). Cell quantification (% mononuclear cells) revealed that sh*Meg3* muscle harbored increased abundance of N-cadherin$^+$ satellite cells, whereas levels of N-cadherin per cell was unchanged (n=3). (B) qPCR expression profiling indicated no change in epithelial markers plakophilin and *Patj*, but mesenchymal markers fibronectin and *Snai2* were significantly upregulated in sh*Meg3* muscle (n=3). (C) Immunofluorescence revealed the presence of satellite cells lacking Snai2 (red arrowheads), Snai2$^+$ satellite cells (white arrowheads), Snai2$^+$ non-satellite cells (green arrowheads) and Snai2$^+$ nuclei in regenerating myofibers (green asterisks). Quantification of Snai2$^+$ cells indicated no change in the occurrence of Snai2$^+$ nuclei (bar graph, % Snai2$^+$ nuclei). Generalized analysis (DAPI) indicated significant upregulation of cytoplasmic Snai2 signal per cell, but no change in nuclear intensity; Snai2 signal in satellite cells (Pax7$^+$) was increased for both cytoplasmic and nuclear compartments (n=3). (D) Immunofluorescence revealed the presence of satellite cells lacking vimentin (red arrowheads), vimentin$^+$ satellite cells (white arrowheads) and vimentin$^+$ non-satellite cells (green arrowheads). Cell quantification (% mononuclear cells) revealed increased abundance of vimentin$^+$ mononucleated cells at both D7 and D14, which could be ascribed to an increase in Pax7$^-$/vimentin$^+$ cells at both timepoints. While Pax7$^+$/vimentin$^+$ cells were modestly reduced at D7, this population was significantly enriched relative to the control at D14. Vimentin signal per cell was downregulated in mononucleated cells at D7, whereas this signal intensity increased at D14 (DAPI), which may reflect sh*Meg3*-specific differences in vimentin$^+$ cell morphology (green channel) (n=3). (E) Sirius Red fibrosis staining on D14 sections revealed increased fibrotic area in sh*Meg3* muscle. (n=3).

Development (2021) 148, dev194027. doi:10.1242/dev.194027

shown to mediate stem cell pluripotency and regulate the differentiation potential of progenitor cells belonging to diverse lineages (Kaneko et al., 2014; Li et al., 2017; Gokey et al., 2018; Yen et al., 2018). Moreover, its depletion activates EMT to promote mesenchymal behavior in cancer cells (Terashima et al., 2017; Deng et al., 2018; Yu et al., 2018). Our findings intersect with these reported functions and demonstrate that *Meg3* is required to prevent inappropriate EMT activation in myoblasts.

EMT is a dynamic process that is not generally associated with muscle differentiation, but the roles of several EMT markers have been independently characterized in myogenic differentiation. The EMT intermediate filament protein vimentin is associated with mesenchymal cell invasiveness, and vimentin facilitates sarcomeric organization by serving as a transient placeholder for muscle-specific desmin during early myogenesis (Gard and Lazarides, 1980). Along these lines, the increased population of vimentin^{+} satellite cells observed in sh*Meg3* day 14 regenerating muscle could indicate delays in sarcomere assembly relative to control. Similarly, TGFβ inhibition resulted in vimentin upregulation in sh*Meg3* C2C12 cells, which correlates with increased myogenic character in these cells.

Snai2 is a major transcriptional regulator of EMT that represses epithelial genes in mesenchymal cells, and during myogenesis Snai2 has been shown to occupy MyoD E-box targets, which has the overall effect of preventing premature differentiation in myoblasts (Hajra et al., 2002; Soleimani et al., 2012). *Meg3*-depleted myoblasts displayed enriched nuclear Snai2 *in vitro* and *in vivo*, and this upregulation was dependent upon TGFβ activity in C2C12 myoblasts. Although EMT is a requisite step for embryonic muscle formation, Snai2 knockdown restored fusion to sh*Meg3* myoblasts, demonstrating these acquired mesenchymal traits must be kept in check to ensure successful cell state transitions for differentiation.

Notably, sh*Meg3* C2C12 cells harbored increased TGFβ and Rho activity, which are not only drivers of EMT, but also potent inhibitors of myogenesis. TGFβ is a potent inhibitor of satellite cell activation (Rathbone et al., 2011), and excessive activity of RhoA, a component of non-canonical TGFβ signaling, has been shown to compromise cell-cell adhesion and fusion competence in myogenic cells (Lu and Krauss, 2010). Enrichment of N-cadherin, a major mediator of EMT, exacerbated the differentiation defects in *Meg3*-depleted myoblasts, as N-cadherin has been shown to trigger RhoA activation (Lovett et al., 2006). Our work indicates that Meg3 modulates repression of antimyogenic EMT-promoting factors TGFβ, RhoA, and Snai2 in myoblasts and injured skeletal muscle to promote myoblast plasticity and differentiation.

PRC2 is an important epigenetic regulator of muscle stem cell identity and myogenic differentiation (Caretti et al., 2004; Juan et al., 2011; Woodhouse et al., 2013), yet there is limited information on how its recruitment is regulated in muscle. Noting that *Meg3* enrichment overlaps with that of Ezh2 in satellite cells (Wüst et al., 2018; Juan et al., 2011), we demonstrate that *Meg3* and Ezh2 interact in proliferating C2C12 myoblasts, and that loss of this interaction perturbs the epigenetic landscape. Given that altered recruitment of Ezh2 facilitated aberrant TGFβ-mediated Snai2 activity and differentiation defects in *Meg3*-depleted myoblasts, *Meg3*-mediated epigenetic repression of TGFβ-related loci represents a nodal regulatory mechanism for fortifying myogenic cell state, and a strong candidate for PRC2 recruitment specificity in myoblasts.

Although *Meg3* is classified as a tumor suppressor, the reduced proliferation caused by its inhibition in myoblasts *in vitro* seems to reflect the context-dependent functions of *Meg3*. Its inhibition resulted in N-cadherin upregulation, which has been shown to suppress cell cycle re-entry in quiescent satellite cells (Goel et al., 2017), and could be further exacerbated by perturbations in Ezh2 function (Juan et al., 2011; Woodhouse et al., 2013). Surprisingly, myoblast proliferation was not affected in regenerating sh*Meg3*-treated muscle, even though aberrant stimulation of TGFβ is an impediment to satellite cell activation and proliferation (Rathbone et al., 2011). Instead, mesenchymal stromal cell (MSC) expansion was observed. Considering MSCs are the only Pax7- interstitial cell population expressing appreciable levels of *Meg3*, we cannot exclude the possibility that *Meg3* knockdown in MSCs triggered this expansion and subsequent fibrosis, suggesting a differential role for *Meg3* in interstitial cell growth. It is noteworthy that mesenchymal stromal cells facilitate regeneration (Wosczyna et al., 2019), but abnormal accumulation of these cells is associated with fibrosis in dystrophic muscle (Ito et al., 2013; Malecova et al., 2018), which could hinder proper allocation of satellite cells during the regenerative process. Future single-cell RNAseq analysis of mononucleated cell populations may provide a deeper understanding of the signaling mechanisms through which *Meg3* regulates muscle and non-muscle cell types in regenerating muscle.

Recently, a subset of *Dlk1-Dio3* miRNAs were shown to suppress age-related atrophy (Shin et al., 2020), and these ncRNAs – including *Meg3* – were markedly downregulated in aged muscle (Mikovic et al., 2018). TGFβ activation is a pathological hallmark for both aged and diseased muscle (Burks and Cohn, 2011), and the fibrotic phenotype of regenerating sh*Meg3*-treated muscle conspicuously resembles age-related muscle-regeneration defects (Beggs et al., 2004; Lukjanenko et al., 2019). Moreover, aged satellite cells accumulate epigenetic abnormalities, such as increased H3K27me3 marks, that suppress their ability to efficiently regenerate muscle (Liu et al., 2013; Sousa-Victor et al., 2014). Given sh*Meg3* myoblasts exhibited abnormal Ezh2 occupancy and H3K27me3 accumulation, we postulate that age-related *Meg3* depletion in muscle induces epigenetic reprogramming that is more prone to pathological TGFβ and EMT signaling. Thus, *Meg3* represents a promising avenue of investigation for therapeutics targeting the deleterious physiology of muscle wasting and dysfunction.

MATERIALS AND METHODS

Cell culture

C2C12 myoblasts were grown and induced to differentiate as described previously (Huang et al., 2006). For stable knockdown, C2C12 myoblasts were seeded at 20-30% confluence in 10 cm format (CELLSTAR) and forward-transfection with Fugene-6 (Promega) according to the manufacturer's protocol with the following plasmids: 9 µg shRNA plasmid (pENTRU6-sh*LacZ* or pENTRU6-sh*Meg3*) and 3 µg pCDNA3 empty vector. For siRNA transfection, 500 ng of Mission siRNA (EMU042121-20UG) were used. For G418 selection, cells were grown in antibiotic-free growth medium supplemented with Geneticin (0.18 mg/ml, Gibco), which was changed daily for 12 days. For heterogeneous studies, cells were used for experiments 48 h after selection. For rescue/overexpression experiments, plates were transfected with 9 µg overexpression plasmid (pShuttleCMV-β-gal or pShuttleCMV-MEG3), 3 µg shRNA plasmid (pENTRU6-sh*LacZ* or pENTR U6-sh*Meg3*) and 1 µg resistance plasmid (pCDNA3 empty vector).

Chromatin immunoprecipitation

On day 3 of differentiation, 30 10 cm plates of C2C12 myotubes were crosslinked by adding freshly prepared p-formaldehyde to a final concentration of 1%. Plates were incubated with gentle shaking at room temperature for exactly 9.5 min, and fixation was quenched with the addition of glycine. Cells were washed twice before collecting pellets with a

Development (2021) 148, dev194027. doi:10.1242/dev.194027

scraper, and pooled by centrifugation. Cross-linked cell pellets were stored at −80, sonicated and examined for chromatin fragment size by gel electrophoresis to confirm 300-700 nucleotide fragments. ChIP was performed as described in the ChIP protocol (Abcam; (https://www.abcam.com/protocols/cross-linking-chromatin-immunoprecipitation-x-chip-protocol). Briefly, 10 µg of H3K27me3 antibody (Abcam 6002), Ezh2 antibody (Millipore 07-689) or normal mouse IgG (Santa Cruz SC2025) was incubated with herring-sperm preadsorbed beads and sonicated overnight at 4°C with nutation. After washing, bead immunoprecipitates were released in ChIP elution buffer with heat and vortexing. Resultant immunoprecipitates and 1% input controls were reverse crosslinked overnight, treated with RNase and proteinase K, and released DNA was subsequently purified by phenol-chloroform extraction and ethanol precipitation. Resultant DNA was resuspended in TE buffer, and 1 µl was used for qPCR reactions and converted to % input.

RNA immunoprecipitation

Sixty 10 cm plates of C2C12 myoblast cell pellets were collected on ice and dounce homogenized in RNase-free AT buffer [20% glycerol, 1 mM EDTA, 0.15 M NaCl, 20 nM HEPES (pH 7.7), DTT, Protease inhibitors, RNAsin]. Equal volumes of cleared lysate were added to 45 µl Protein G beads (Santa Cruz SC2002) preincubated with 0.5 µl Ezh2 antibody (Millipore 07-689) or normal mouse IgG (Santa Cruz SC2025). Following overnight nutation at 4°C, 45 µl supernatant was collected for normalization control and immunoprecipitates were washed four times with AT buffer before resuspending bead conjugates in Trizol for RNA purification.

cDNA synthesis and qPCR

RNA from C2C12 myoblasts or TA muscle was extracted with Trizol Reagent (Ambion) and used according to manufacturer's protocol. RNA template was converted to cDNA using M-MLV reverse transcriptase, random oligo dT primers and RNAs in according with the manufacturer's protocol (Promega). Quantitative RT-PCR was performed in triplicate wells using Power SYBR Green Master Mix (Applied Biosystems) with the 7900HT Sequence Detection System (Applied Biosystems). Primers used for all qRT-PCR expression profiling analyses are listed in Table S1. Primers for ChIP-qPCR are provided in Table S2A,B.

Plasmids

For overexpression, human *MEG3* cDNA was PCR amplified from the pCI-Meg3 (Addgene Plasmid #44727) using NEB Q5 high-fidelity polymerase, and cloned into pShuttleCMV vector (Agilent AdEasy Adenoviral Vector System). For knockdown, the sh*Meg3* target sequence was derived from Mondal et al. (2015) and a double-stranded RNA insert was ligated to the U6-pENTR shuttle vector (BLOCK-iT U6 RNAi Entry Vector Kit, Invitrogen). Construction of sh*LacZ* has been described previously (Ewen et al., 2011). Plasmids were grown in DH5α cells and purified using midi-prep columns (Machery-Nagel Nucleobond).

Adenovirus

To generate Adenoviruses used for muscle regeneration, pENTR U6-shRNA plasmids or pCMV-transgene plasmids were ligated to pAd plasmid and transfected into HEK293A cells. The Notch-ICD and Shh-N adenoviruses were generously provided by Igor Prudovsky (Maine Medical Center Research Institute) and Ronald G. Crystal (Cornell Medical Center), respectively. Following plaque formation, crude viral lysates were precipitated and purified by CsCl purification and dialysis. Virus was titered by serial dilution and plaque formation. All *in vitro* adenoviral transductions were performed 48 h prior to differentiation with an MOI of 25, with the exception of MEG3, which was used at an MOI of 60.

Muscle injury

Tibialis anterior (TA) muscles of Swiss-Webster mice (female, 25 grams, Taconic) were injected with 10 µM cardiotoxin (*Naja nigricollis,* EMD chemicals) in saline solution containing 5×10^{10} pfus adenovirus, and administered as 50 µl injections per TA muscle. An additional round of virus was injected 24 h post-CTX injury and muscles were harvested 3, 7 and 14 days post-injury.

Inhibitors and growth factors

All chemical inhibitors were resuspended according to the manufacturer's recommendations and added to cells at the indicated concentration by diluting with culture medium. For myoblast treatments, subconfluent cells were treated 48 h prior to analyses. For mygenic differentiation, inhibitors were added at specific times relative to the onset of differentiation as follows: Unc1999 was added 24 h prior to differentiation and washed away upon changing to differentiation medium; pifithrin-α hydrobromide (Pifithrin) was added once, 40 min prior to differentiation, and washed away upon changing to differentiation medium; all other chemical inhibitors were added to media on the days of seeding (day −1) and differentiation (day 0). Media were replaced daily (with one wash) to circumvent degradation. Final concentrations: pifithrin-α hydrobromide (30 µM, Tocris), LY2157299 (10 µM, Sigma), Y-27632 (40 µM Sigma), SB203580 (10 µM, Calbiochem), SIS3 (5 µM, Calbiochem), BMP4 (50 ng/µl Life Technologies) and Unc1999 (2 µM Sigma).

Immunofluorescence

C2C12 myoblasts and transverse TA muscle cryosections (16 µm) were post-fixed with 4% para-formaldehyde and blocked with PBS solution containing 0.3% Triton-X 100 and 3% normal donkey serum (Sigma). Antibody dilution buffer consisted of PBS containing 1% BSA and 0.3% Triton-X 100, and samples were immunostained as described by Kanisiack et al. (2009). Primary antibodies were for: MYH4 (1:200, Proteintech 20140-1-AP), α-actinin (1:1000, Sigma A7811), BrdU (1:500, Invitrogen MoBU-1), Ki67 (1:2000, Abcam ab15580), laminin (1:2000, Sigma L9393), Pax7 (1:200, DSHB PAX7), PDGFRα (1:200, Proteintech 60045-1-Ig), Cdh1 (1:500, Abcam ab40772), Cdh2 (1:500, Abcam ab76011), Snai2/Slug (1:500, Abcam ab85936) and vimentin (1:1000, Abcam ab92547). Secondary antibodies were: donkey anti-mouse Alexa-Fluor 488 IgG (1:2000, Invitrogen A21202), donkey anti-mouse Alexa-Fluor 568 IgG (1:2000, Invitrogen A10037), donkey anti-rabbit Alexa-Fluor 488 IgG (1:2000, Invitrogen A21206) and donkey anti-rabbit Alexa-Fluor 555 IgG (1:2000, Invitrogen A31572). All samples were mounted with DAPI Vectashield mounting medium. For Pax7 immunostaining, immunostaining was modified to follow protocol for Mouse on Mouse Immunodetection kit (Abcam). For BrdU, proliferating C2C12 myoblasts were pulsed with 10µM BrdU (BD Pharmingen) for 60 min followed by fixation, incubated with 2.5 M HCl solution at 37°C for 20 min, and washed four times with PBS prior to immunostaining.

MitoTrackerCMXRos

MitoTracker reagent (Invitrogen M7512) was resuspended in DMSO according to the manufacturer's protocol and added to C2C12 cultures to a final concentration of 50 µM. Following 30 min incubation, cells were fixed and subjected to immunostaining.

Image acquisition

BrdU- and laminin-stained images were acquired using an Olympus DSU BX61 (BU Proteomics and Imaging Core). Bright-field images for scratch-wound assays (Figure 5D) were acquired using an Olympus IX50 (BU Proteomics and Imaging Core). All other immunofluorescent and bright-field images were captured using a Nikon Eclipse NiE (BU Proteomics and Imaging Core).

Image analyses

The fusion index was quantified using the ImageJ Cell Counter Plugin. Immunofluorescence was measured on ImageJ using the Intensity Ratio Nuclei Cytoplasm Tool (http://dev.mri.cnrs.fr/projects/imagej-macros/wiki/Intensity_Ratio_Nuclei_Cytoplasm_Tool). Scratch wound assay scratch areas were measured with the MRI Wound Healing Tool (https://github.com/MontpellierRessourcesImagerie/imagej_macros_and_scripts/wiki/Wound-Healing-Tool). Cross-sectional area (CSA) of skeletal muscle was assessed in laminin-stained sections using ImageJ threshold, binary and watershed functions, and area tracing tools. The Sirius Red fibrotic area was measured using the Fibrosis tool plug-in with custom color deconvolution. (https://github.com/MontpellierRessourcesImagerie/imagej_macros_and_scripts/wiki/MRI_Fibrosis_Tool).

RNA-sequencing

RNA samples corresponding to day 3 C2C12 differentiation (n=3 sh*LacZ*, n=3 sh*Meg3*) and day 7 injured TA muscle (n=3 sh*LacZ*, n=3 sh*Meg3*) were submitted to the Boston University Microarray and Sequencing Resource Core for library prep and Illumina sequencing. Single cell RNA-seq data were obtained from the FACS data visualization, provided by the Chan-Zuckerburg Initiative BioHub (https://tabula-muris.ds.czbiohub.org/). Permission to use BioHub data in Fig. 1 was granted by Tabula Muris corresponding author Spyros Darmanis.

Western blot analysis

C2C12 cells were lysed by dounce-homogenization in the presence of ELB with DTT and protease inhibitors. Protein concentration was determined by Bradford assay (Bio-Rad, 500-0006). Western blots were performed as previously described (McCalmon et al., 2010), with the following modifications: primary antibodies were incubated overnight in BLOTTO solution at 4°C; subsequent washes were gradually transitioned to PBS for 1 h Licor dye incubation; and membranes were shielded from light and pressed dry with Whatman paper prior to image acquisition (Azure Sapphire Biomolecular Imager). Primary antibodies against the following proteins were used: β-tubulin (1:5000, Cell Signaling Technology mAb #3873), MF20 (0.2 µg/ml, DSHB MF-20 supernatant), Cdh1 (1:1000, Abcam ab40772), Cdh2 (1:1000, Abcam ab76011), Vimentin (1:2000, Abcam ab92547). Secondary dyes used were rabbit 800 (1:2000, Licor 926-32211) and mouse 680 (1:2000, Licor 926-68070).

Statistical analysis

All numerical quantification is represented as mean±s.e.m. of at least three independently performed experiments. Statistically significant differences between two populations of data were determined using Student's t-test. $P \leq 0.05$ was considered to be statistically significant ($^{*}P<0.05$, $^{**}P<0.01$, $^{***}P<0.001$, for Student's t-test). When more than one treatment was performed, samples were examined by ANOVA (one-way) to confirm differences were present; if $P<0.05$, Student's t-test was performed post-hoc comparing each treatment group to the no-treatment control. Bar graph data are presented as mean±s.e.m.

Acknowledgements

We are grateful to the BU Sequencing Core for RNA-sequencing and to Adam Gower for bioinformatics analysis. We also thank Andrew Emili (Director, Center for Systems Biology, BU School of Medicine) and Angela Ho (BU Department of Biology) for providing us with additional reagents and advice, and Heather Hook, Tarik Zahr and Roxanna Altus for excellent technical assistance.

Competing interests

The authors declare no competing or financial interests.

Author contributions

Conceptualization: T.L.D., F.J.N.; Methodology: T.L.D., F.J.N.; Validation: T.L.D., F.J.N.; Formal analysis: T.L.D., A.C., A.P., J.G., F.J.N.; Investigation: T.L.D., A.C., A.P., J.G., F.J.N.; Resources: T.L.D., F.J.N.; Data curation: T.L.D., A.C., A.P., F.J.N.; Writing - original draft: T.L.D., F.J.N.; Writing - review & editing: T.L.D., F.J.N.; Visualization: T.L.D., F.J.N.; Supervision: T.L.D., F.J.N.; Project administration: F.J.N.; Funding acquisition: F.J.N.

Funding

This work was supported in part by a National Science Foundation Graduate Research Fellowship Program grant to T.L.D., by a Boston University-CTSI Core Voucher and by funds provided by Boston University.

Data availability

RNA-seq data from this study are available in the Dryad Digital Repository (Naya et al., 2020): dryad.k0p2ngf77.

Supplementary information

Supplementary information available online at
https://dev.biologists.org/lookup/doi/10.1242/dev.194027.supplemental

Peer review history

The peer review history is available online at
https://dev.biologists.org/lookup/doi/10.1242/dev.194027.reviewer-comments.pdf

References

Beggs, M. L., Nagarajan, R., Taylor-Jones, J. M., Nolen, G., Macnicol, M. and Peterson, C. A. (2004). Alterations in the TGFβ signaling pathway in myogenic progenitors with age. *Aging Cell.* **3**:353-361. doi:10.1111/j.1474-9728.2004.00135.x

Benetatos, L., Hatzimichael, E., Londin, E., Vartholomatos, G., Loher, P., Rigoutsos, I. and Briasoulis, E. (2013). The microRNAs within the DLK1-DIO3 genomic region: involvement in disease pathogenesis. *Cell. Mol. Life Sci.* **70**, 795-814. doi:10.1007/s00018-012-1080-8

Benetatos, L., Vartholomatos, G. and Hatzimichael, E. (2014). DLK1-DIO3 imprinted cluster in induced pluripotency: landscape in the mist. *Cell. Mol. Life Sci.* **71**, 4421-4430. doi:10.1007/s00018-014-1698-9

Buckingham, M. and Rigby, P. W. (2014). Gene regulatory networks and transcriptional mechanisms that control myogenesis. *Dev. Cell* **28**, 225-238. doi:10.1016/j.devcel.2013.12.020

Burks, T. N. and Cohn, R. D. (2011). Role of TGF-β signaling in inherited and acquired myopathies. *Skelet Muscle.* **1**:19. doi:10.1186/2044-5040-1-19

Campbell, K. and Casanova, J. (2016). A common framework for EMT and collective cell migration. *Development.* **143**, 4291-4300. doi:10.1242/dev.139071

Caretti, G., Di Padova, M., Micales, B., Lyons, G. E. and Sartorelli, V. (2004). The Polycomb Ezh2 methyltransferase regulates muscle gene expression and skeletal muscle differentiation. *Genes Dev.* **18**:2627-2638. doi:10.1101/gad.1241904

Castel, D., Baghdadi, M. B., Mella, S., Gayraud-Morel, B., Marty, V., Cavaillé, J., Antoniewski, C. and Tajbakhsh, S. (2018). Small-RNA sequencing identifies dynamic microRNA deregulation during skeletal muscle lineage progression. *Sci. Rep.* **8**, 4208. doi:10.1038/s41598-018-21991-w

Chal, J. and Pourquié, O. (2017). Making muscle: skeletal myogenesis in vivo and in vitro. *Development* **144**, 2104-2122. doi:10.1242/dev.151035

da Rocha, S. T., Edwards, C. A., Ito, M., Ogata, T. and Ferguson-Smith, A. C. (2008). Genomic imprinting at the mammalian Dlk1-Dio3 domain. *Trends Genet.* **24**, 306-316. doi:10.1016/j.tig.2008.03.011

Das, P. P., Hendrix, D. A., Apostolou, E., Buchner, A. H., Canver, M. C. and Orkin, S. (2015). PRC2 is required to maintain expression of the maternal Gtl2-rian-mirg locus by preventing De Novo DNA methylation in mouse embryonic stem cells. *Cell Rep* **12**, 1456-1470. doi:10.1016/j.celrep.2015.07.053

Deng, R., Fan, F. Y., Yi, H., Liu, F., He, G. C., Sun, H. P. and Su, Y. (2018). MEG3 affects the progression and chemoresistance of T-cell lymphoblastic lymphoma by suppressing epithelial-mesenchymal transition via the PI3K/mTOR pathway. *J. Cell. Biochem.* **120**, 8144-8153. doi:10.1002/jcb.28093

Dill, T. L. and Naya, F. J. (2018). A hearty dose of noncoding RNAs: the imprinted DLK1-DIO3 locus in cardiac development and disease. *J. Cardiovasc. Dev. Dis.* **5**, 37. doi:10.3390/jcdd5030037

Eisenberg, I., Eran, A., Nishino, I., Moggio, M., Lamperti, C., Amato, A. A., Lidov, H. G., Kang, P. B., North, K. N., Mitrani-Rosenbaum, S. et al. (2007). Distinctive patterns of microRNA expression in primary muscular disorders. *Proc. Nat. Acad. Sci. USA* **104**, 17016-17021. doi:10.1073/pnas.0708115104

Ewen, E. P., Snyder, C. M., Wilson, M., Desjardins, D. and Naya, F. J. (2011). The Mef2A transcription factor coordinately regulates a costamere gene program in cardiac muscle. *J. Biol. Chem.* **286**:29644-29653. doi:10.1074/jbc.M111.268094

Gao, Y.-Q., Chen, X., Wang, P., Lu, L., Zhao, W., Chen, C., Chen, C.-P., Tao, T., Sun, J., Zheng, Y.-Y. et al. (2015). Regulation of DLK1 by the maternally expressed miR-379/miR-544 cluster may underlie callipyge polar overdominance inheritance. *Proc. Natl. Acad. Sci. USA* **112**:13627-13632. doi:10.1073/pnas.1511448112

Gard, D. L. and Lazarides, E. (1980). The synthesis and distribution of desmin and vimentin during myogenesis in vitro. *Cell* **19**, 263-275. doi:10.1016/0092-8674(80)90408-0

Goel, A. J., Rieder, M. K., Arnold, H. H., Radice, G. L. and Krauss, R. S. (2017). Niche cadherins control the quiescence-to-activation transition in muscle stem cells. *Cell Rep.* **21**:2236-2250. doi:10.1016/j.celrep.2017.10.102

Gokey, J. J., Snowball, J., Sridharan, A., Speth, J. P., Black, K. E., Hariri, L. P., Perl, A. T., Xu, Y. and Whitsett, J. A. (2018). MEG3 is increased in idiopathic pulmonary fibrosis and regulates epithelial cell differentiation. *JCI Insight.* **3**: e122490. doi:10.1172/jci.insight.122490

Haga, C. L. and Phinney, D. G. (2012). MicroRNAs in the imprinted DLK1-DIO3 region repress the epithelial-to-mesenchymal transition by targeting the TWIST1 protein signaling network. *J. Biol. Chem.* **287**, 42695-42707. doi:10.1074/jbc.M112.387761

Hajra, K. M., Chen, D. Y. and Fearon, E. R. (2002). The SLUG zinc-finger protein represses E-cadherin in breast cancer. *Cancer Res.* **62**:1613-1618.

Huang, H. T., Brand, O. M., Mathew, M., Ignatiou, C., Ewen, E. P., McCalmon, S. A. and Naya, F. J. (2006). Myomaxin is a novel transcriptional target of MEF2A that encodes a Xin-related α-actinin-interacting protein. *J. Biol. Chem.* **281**:39370-39379. doi:10.1074/jbc.M603244200

Ioannides, Y., Lokulo-Sodipe, K., Mackay, D. J., Davies, J. H. and Temple, I. K. (2014). Temple syndrome: improving the recognition of an underdiagnosed chromosome 14 imprinting disorder: an analysis of 51 published cases. *J. Med. Genet.* **51**:495-501. doi:10.1136/jmedgenet-2014-102396

Ito, T., Ogawa, R., Uezumi, A., Ohtani, T., Watanabe, Y., Tsujikawa, K., Miyagoe-Suzuki, Y., Takeda, S., Yamamoto, H. and Fukada, S. (2013). Imatinib attenuates severe mouse dystrophy and inhibits proliferation and fibrosis-marker

expression in muscle mesenchymal progenitors. *Neuromuscul. Disord.* **23**, 349-356. doi:10.1016/j.nmd.2012.10.025

Joe, A. W., Yi, L., Natarajan, A., Le Grand, F., So, L., Wang, J., Rudnicki, M. A. and Rossi, F. M. (2010). Muscle injury activates resident fibro/adipogenic progenitors that facilitate myogenesis. *Nat. Cell Biol.* **12**:153-163. doi:10.1038/ncb2015

Juan, A. H., Derfoul, A., Feng, X., Ryall, J. G., Dell'Orso, S., Pasut, A., Zare, H., Simone, J. M., Rudnicki, M. A. and Sartorelli, V. (2011). Polycomb EZH2 controls self-renewal and safeguards the transcriptional identity of skeletal muscle stem cells. *Genes Dev.* **25**, 789-794. doi:10.1101/gad.2027911

Kameswaran, V., Bramswig, N. C., McKenna, L. B., Penn, M., Schug, J., Hand, N. J., Chen, Y., Choi, I., Vourekas, A., Won, K. J. et al. (2014). Epigenetic regulation of the DLK1-MEG3 microRNA cluster in human type 2 diabetic islets. *Cell Metab.* **19**:135-145. doi:10.1016/j.cmet.2013.11.016

Kaneko, S., Bonasio, R., Saldaña-Meyer, R., Yoshida, T., Son, J., Nishino, K., Umezawa, A. and Reinberg, D. (2014). Interactions between JARID2 and noncoding RNAs regulate PRC2 recruitment to chromatin. *Mol. Cell* **53**, 290-300. doi:10.1016/j.molcel.2013.11.012

Kanisicak, O., Mendez, J. J., Yamamoto, S., Yamamoto, M. and Goldhamer, D. J. (2009). Progenitors of skeletal muscle satellite cells express the muscle determination gene, MyoD. *Dev. Biol.* **332**:131-141. doi:10.1016/j.ydbio.2009.05.554

Kollias, H. D. and McDermott, J. C. (2008). Transforming growth factor-beta and myostatin signaling in skeletal muscle. *J. Appl. Physiol.* **104**:579-587. doi:10.1152/japplphysiol.01091.2007

Krauss, R. S. (2010). Regulation of promyogenic signal transduction by cell-cell contact and adhesion. *Exp. Cell Res.* **316**:3042-3049. doi:10.1016/j.yexcr.2010.05.008

Labialle, S., Marty, V., Bortolin-Cavaillé, M. L., Hoareau-Osman, M., Pradère, J. P., Valet, P., Martin, P. G. and Cavaillé, J. (2014). The miR-379/miR-410 cluster at the imprinted Dlk1-Dio3 domain controls neonatal metabolic adaptation. *EMBO J.* **33**, 2216-2230. doi:10.15252/embj.201387038

Lamouille, S., Xu, J. and Derynck, R. (2014). Molecular mechanisms of epithelial-mesenchymal transition. *Nat. Rev. Mol. Cell Biol.* **15**, 178-196. doi:10.1038/nrm3758

Li, Z., Jin, C., Chen, S., Zheng, Y., Huang, Y., Jia, L., Ge, W. and Zhou, Y., Long non-coding RNA (2017). MEG3 inhibits adipogenesis and promotes osteogenesis of human adipose-derived mesenchymal stem cells via miR-140-5p. *Mol. Cell. Biochem.* **433**:51-60. doi:10.1007/s11010-017-3015-z

Liu, L., Luo, G.-Z., Yang, W., Zhao, X., Zheng, Q., Lv, Z., Li, W., Wu, H.-J., Wang, L., Wang, X.-J. et al. (2010). Activation of the imprinted Dlk1-Dio3 region correlates with pluripotency levels of mouse stem cells. *J. Biol. Chem.* **285**, 19483-19490. doi:10.1074/jbc.M110.131995

Liu, L., Cheung, T. H., Charville, G. W., Hurgo, B. M., Leavitt, T., Shih, J., Brunet, A. and Rando, T. A. (2013). Chromatin modifications as determinants of muscle stem cell quiescence and chronological aging. *Cell Rep.* **4**:189-204. doi:10.1016/j.celrep.2013.05.043

Lovett, F., Gonzalez, I., Salih, D., Cobb, L., Tripathi, G., Cosgrove, R., Murrell, A., Kilshaw, J. and Pell, J. (2006). Convergence of Igf2 expression and adhesion signalling via RhoA and p38 MAPK enhances myogenic differentiation. *J Cell Science.* **119**, 4828-4840. doi:10.1242/jcs.03278

Lu, M. and Krauss, R. (2010). Abl promotes cadherin-dependent adhesion and signaling in myoblasts. *Cell Cycle.* **9**, 2737-2741. doi:10.4161/cc.9.14.12246

Lukjanenko, L., Karaz, S., Stuelsatz, P., Gurriaran-Rodriguez, U., Michaud, J., Dammone, G., Sizzano, F., Mashinchian, O., Ancel, S., Migliavacca, E. et al. (2019). Aging disrupts muscle stem cell function by impairing matricellular WISP1 secretion from fibro-adipogenic progenitors. *Cell Stem Cell.* **24**:433-446. doi:10.1016/j.stem.2018.12.014

Luo, Z., Lin, C., Woodfin, A. R., Bartom, E. T., Gao, X., Smith, E. R. and Shilatifard, A. (2016). Regulation of the imprinted Dlk1-Dio3 locus by allele-specific enhancer activity. *Genes Dev.* **30**, 92-101. doi:10.1101/gad.270413.115

Malecova, B., Gatto, S., Etxaniz, U., Passafaro, M., Cortez, A., Nicoletti, C., Giordani, L., Torcinaro, A., De Bardi, M., Bicciato, S. et al. (2018). Dynamics of cellular states of fibro-adipogenic progenitors during myogenesis and muscular dystrophy. *Nat. Commun.* **9**:3670. doi:10.1038/s41467-018-06068-6

McCalmon, S. A., Desjardins, D. M., Ahmed, S., Davidoff, K. S., Synder, C. M., Sato, K., Ohashi, K., Kielbasa, O. M., Mathew, M., Ewen, E. P. et al. (2010). Modulation of angiotensin II-mediated cardiac remodeling by the MEF2A target gene Xirp2. *Circ. Res.* **106**, 952-960. doi:10.1161/CIRCRESAHA.109.209007

Mikovic, J., Sadler, K., Butchart, L., Voisin, S., Gerlinger-Romero, F., Della Gatta, P., Grounds, M. D. and Lamon, S. (2018). MicroRNA and long non-coding RNA regulation in skeletal muscle from growth to old age shows striking dysregulation of the callipyge locus. *Front. Genet.* **9**:548. doi:10.3389/fgene.2018.00548

Mondal, T., Subhash, S., Vaid, R., Enroth, S., Uday, S., Reinius, B., Mitra, S., Mohammed, A., James, A. R., Hoberg, E. et al. (2015). MEG3 long noncoding RNA regulates the TGF-β pathway genes through formation of RNA-DNA triplex structures. *Nat. Commun.* **6**, 7743. doi:10.1038/ncomms8743

Naya, F., Dill, T., Carroll, A., Pinhiero, A. and Gao, J. (2020). Transcriptomic data and analyses of shMeg3 muscle in vitro and in vivo. *Dryad Digital Repository* doi:10.5061/dryad.k0p2ngf77

Nishiyama, T., Kii, I. and Kudo, A. (2004). Inactivation of Rho/ROCK signaling is crucial for the nuclear accumulation of FKHR and myoblast fusion. *J. Biol. Chem.* **279**, 47311-47319. doi:10.1074/jbc.M403546200

Ogata, T., Kagami, M. and Ferguson-Smith, A. C. (2008). Molecular mechanisms regulating phenotypic outcome in paternal and maternal uniparental disomy for chromosome 14. *Epigenetics.* **3**:181-187. doi:10.4161/epi.3.4.6550

Qian, P., He, X. C., Paulson, A., Li, Z., Tao, F., Perry, J. M., Guo, F., Zhao, M., Zhi, L., Venkatraman, A. et al. (2016). The Dlk1-Gtl2 locus preserves LT-HSC function by inhibiting the PI3K-mTOR pathway to restrict mitochondrial metabolism. *Cell Stem Cell.* **18**, 214-228. doi:10.1016/j.stem.2015.11.001

Rathbone, C. R., Yamanouchi, K., Chen, X. K., Nevoret-Bell, C. J., Rhoads, R. P. and Allen, R. E. (2011). Effects of transforming growth factor-beta (TGF-β1) on satellite cell activation and survival during oxidative stress. *J. Muscle Res. Cell Motil.* **32**:99-109. doi:10.1007/s10974-011-9255-8

Sartori, R., Schirwis, E., Blaauw, B., Bortolanza, S., Zhao, J., Enzo, E., Stantzou, A., Mouisel, E., Toniolo, L., Ferry, A. et al. (2013). BMP signaling controls muscle mass. *Nat. Genet.* **45**, 1309-1318. doi:10.1038/ng.2772

Schaum, N., Karkanias, J., Neff, N. F., May, A. P., Quake, S. R., Wyss-Coray, T., Darmanis, S., Batson, J., Botvinnik, O. and Chen, M. B. (2018). Single-cell transcriptomics of 20 mouse organs creates a *Tabula Muris*. *Nature* **562**, 367-372. doi:10.1038/s41586-018-0590-4

Segalés, J., Perdiguero, E. and Muñoz-Cánoves, P. (2016). Regulation of muscle stem cell functions: a focus on the p38 MAPK signaling pathway. *Front Cell Dev Biol.* **4**, 91. doi:10.3389/fcell.2016.00091

Shin, Y. J., Kwon, E. S., Lee, S. M., Kim, S. K., Min, K. W., Lim, J. Y., Lee, B., Kang, J. S., Kwak, J. Y., Son, Y. H. et al. (2020). A subset of microRNAs in the Dlk1-Dio3 cluster regulates age-associated muscle atrophy by targeting Atrogin-1. *J Cachexia Sarcopenia Muscle* **11**, 1336-1350. doi:10.1002/jcsm.12578

Snyder, C. M., Rice, A., Estrella, N., Held, A., Kandarian, S. C. and Naya, F. J. (2013). MEF2A regulates the Gtl2-Dio3 microRNA mega-cluster to modulate WNT signaling in skeletal muscle regeneration. *Development* **140**, 31-42. doi:10.1242/dev.081851

Soleimani, V. D., Yin, H., Jahani-Asl, A., Ming, H., Kockx, C. E., van Ijcken, W. F., Grosveld, F. and Rudnicki, M. A. (2012). Snail regulates MyoD binding-site occupancy to direct enhancer switching and differentiation-specific transcription in myogenesis. *Mol. Cell* **47**:457-468. doi:10.1016/j.molcel.2012.05.046

Sousa-Victor, P., Gutarra, S., García-Prat, L., Rodriguez-Ubreva, J., Ortet, L., Ruiz-Bonilla, V., Jardí, M., Ballestar, E., González, S., Serrano, A. L. et al. (2014). Geriatric muscle stem cells switch reversible quiescence into senescence. *Nature* **506**, 316-321. doi:10.1038/nature13013

Stadtfeld, M., Apostolou, E., Akutsu, H., Fukuda, A., Follett, P., Natesan, S., Kono, T., Shioda, T. and Hochedlinger, K. (2010). Aberrant silencing of imprinted genes on chromosome 12qF1 in mouse induced pluripotent stem cells. *Nature* **465**, 175-181. doi:10.1038/nature09017

Terashima, M., Tange, S., Ishimura, A. and Suzuki, T. (2017). MEG3 long noncoding RNA contributes to the epigenetic regulation of epithelial-mesenchymal transition in lung cancer cell lines. *J. Biol. Chem.* **292**, 82-99. doi:10.1074/jbc.M116.750950

Tierling, S., Dalbert, S., Schoppenhorst, S., Tsai, C. E., Oliger, S., Ferguson-Smith, A. C., Paulsen, M. and Walter, J. (2006). High-resolution map and imprinting analysis of the Gtl2-Dnchc1 domain on mouse chromosome 12. *Genomics.* **87**, 225-235. doi:10.1016/j.ygeno.2005.09.018

Uezumi, A., Ikemoto-Uezumi, M. and Tsuchida, K. (2014). Roles of nonmyogenic mesenchymal progenitors in pathogenesis and regeneration of skeletal muscle. *Front. Physiol.* **5**, 68. doi:10.3389/fphys.2014.00068

Ungefroren, H., Witte, D. and Lehnert, H. (2018). The role of small GTPases of the Rho/Rac family in TGF-β-induced EMT and cell motility in cancer. *Dev. Dyn.* **247**, 451-461. doi:10.1002/dvdy.24505

Woodhouse, S., Pugazhendhi, D., Brien, P. and Pell, J. M. (2013). Ezh2 maintains a key phase of muscle satellite cell expansion but does not regulate terminal differentiation. *J. Cell Sci.* **126**:565-579. doi:10.1242/jcs.114843

Wosczyna, M. N. and Rando, T. A. (2018). A muscle stem cell support group: coordinated cellular responses in muscle regeneration. *Dev. Cell* **46**:135-143. doi:10.1016/j.devcel.2018.06.018

Wosczyna, M. N., Konishi, C. T., Perez Carbajal, E. E., Wang, T. T., Walsh, R. A., Gan, Q., Wagner, M. W. and Rando, T. A. (2019). Mesenchymal stromal cells are required for regeneration and homeostatic maintenance of skeletal muscle. *Cell Rep.* **27**:2029-2035. doi:10.1016/j.celrep.2019.04.074

Wüst, S., Dröse, S., Heidler, J., Wittig, I., Klockner, I., Franko, A., Bonke, E., Günther, S., Gärtner, U., Boettger, T. et al. (2018). Metabolic maturation during muscle stem cell differentiation is achieved by miR-1/133a-mediated inhibition of the Dlk1-Dio3 mega gene cluster. *Cell Metab.* **27**, 1026-1039. doi:10.1016/j.cmet.2018.02.022

Yen, Y.-P., Hsieh, W.-F., Tsai, Y.-Y., Lu, Y.-L., Liau, E. S., Hsu, H.-C., Chen, Y.-C., Liu, T.-C., Chang, M., Li, J. et al. (2018). Dlk1-Dio3 locus-derived lncRNAs perpetuate postmitotic motor neuron cell fate and subtype identity. *eLife* **7**, e38080. doi:10.7554/eLife.38080

Yu, F., Geng, W., Dong, P., Huang, Z. and Zheng, J. (2018). LncRNA-MEG3 inhibits activation of hepatic stellate cells through SMO protein and miR-212. *Cell Death Dis.* **9**, 1014. doi:10.1038/s41419-018-1068-x

Yusuf, F. and Brand-Saberi, B. (2006). The eventful somite: patterning, fate determination and cell division in the somite. *Anat. Embryol. (Berl)* **211**, 21-30. doi:10.1007/s00429-006-0119-8

Zhao, J., Ohsumi, T. K., Kung, J. T., Ogawa, Y., Grau, D. J., Sarma, K., Song, J. J., Kingston, R. E., Borowsky, M. and Lee, J. T. (2010). Genome-wide

identification of polycomb-associated RNAs by RIP-seq. *Mol. Cell* **40**, 939-953. doi:10.1016/j.molcel.2010.12.011

Zhou, Y., Zhong, Y., Wang, Y., Zhang, X., Batista, D. L., Gejman, R., Ansell, P. J., Zhao, J., Weng, C. and Klibanski, A. (2007). Activation of p53 by MEG3 non-coding RNA. *J. Biol. Chem.* **282**, 24731-24742. doi:10.1074/jbc.M702029200

Zhou, Y., Cheunsuchon, P., Nakayama, Y., Lawlor, M. W., Zhong, Y., Rice, K. A., Zhang, L., Zhang, X., Gordon, F. E., Lidlov, H. G. W. et al. (2010). Activation of paternally expressed genes and perinatal death caused by deletion of the *Gtl2* gene. *Development* **137**, 2643-2652. doi:10.1242/dev.045724